Sensitivity analysis of an updated bidirectional air-surface exchange model for elemental mercury vapor

Xun Wang[1,2], Che-Jen Lin[1,3,4], Xinbin Feng[1]

[1] State Key Laboratory of Environmental Geochemistry, Institute of Geochemistry, Chinese Academy of Sciences, Guiyang, China

[2] University of Chinese Academy of Sciences, Beijing, China

[3] Department of Civil Engineering, Lamar University, Beaumont, TX, USA

[4] College of Environment and Energy, South China University of Technology, Guangzhou, China

Correspondence to: C.-J. Lin (jerry.lin@lamar.edu); X. Feng (fengxinbin@vip.skleg.cn)

Abstract

A box model for estimating bidirectional air-surface exchange of gaseous elemental mercury (Hg^0) has been updated based on the latest understanding of the resistance scheme of atmosphere-biosphere interface transfer. Simulations were performed for two seasonal months to evaluate diurnal and seasonal variation. The base-case results show that water and soil surfaces are net sources while vegetation is a net sink of Hg^0. The estimated net exchange in a domain covering the contiguous US and part of Canada and Mexico is 38 and 56 Mg as evasion in the summer and winter month. The smaller evasion in summer is due to the stronger Hg^0 uptake by vegetation. Modeling experiments using a 2-level factorial design were conducted to examine the sensitivity of flux response to changes of physical and environmental parameters in the model. It is shown that atmospheric shear flows (surface wind over water and friction velocity over terrestrial surfaces), dissolved gaseous mercury (DGM) concentration, soil organic and Hg content, and air temperature are the most influential factors. The positive effect of friction velocity and

soil Hg content on the evasion flux from soil and canopy can be effectively offset by the negative effect of soil organic content. Significant synergistic effects are identified between surface wind and DGM level for water surface, and between soil Hg content and friction velocity for soil surface, leading to ~50% enhanced flux compared to the sum of their individual effects. The air-foliar exchange is mainly controlled by surface resistance terms influenced by solar irradiation and air temperature. Research in providing geospatial distribution of Hg in water and soil will greatly improve the flux estimate. Elucidation on the kinetics and mechanism of Hg(II) reduction in soil/water and quantification of the surface resistances specific to Hg species will also help reduce the model uncertainty.

1 Introduction

Mercury (Hg) is a persistent, bioaccumulative pollutant released into the atmosphere from a variety of anthropogenic and natural sources. The anthropogenic release (2000~2400 Mg yr^{-1}) primarily comes from fossil fuel combustion, waste incineration, metal smelting and cement production (Pacyna et al., 2006;Pacyna et al., 2003;Streets et al., 2005;Streets et al., 2009;Pirrone et al., 2010). The natural sources include geological weathering from Hg enriched substrates, biomass burning, volcanic activities and other Hg^0 exchange, including so-called re-emission, at the atmosphere-biosphere interface (Gustin et al., 2008;Mason and Sheu, 2002). While the men-made emissions have been estimated and continuously updated with reasonable consistency since the 1990s, the estimates for natural emissions have been highly uncertain (1500-5207 Mg yr^{-1}), primarily due to a lack of understanding in the air-surface exchange of Hg^0. Since the natural release can account for up to two-thirds of global mercury input to the atmosphere (Friedli et al., 2009;Pirrone et al., 2010), better quantification of the mass input is critical in assessing the global biogeochemical cycling of mercury (Lindberg et al., 2007).

Air-surface exchange is an important component in atmospheric mercury modeling for estimating Hg^0 evasion and deposition over soil, water and vegetation. For terrestrial surfaces, the soil Hg evasion has

been calculated using the statistical relationships obtained from the measured Hg^0 flux and observed environmental factors such as temperature, solar irradiance, leaf area index, and Hg content (Bash et al., 2004;Gbor et al., 2006;Lin et al., 2005;Shetty et al., 2008;Xu et al., 1999;Selin and Jacob, 2008;Smith-Downey et al., 2010). Such an approach oversimplifies the role of environmental factors in the exchange process because Hg^0 flux was measured only in a limited number of locations where the environmental parameters (such as soil properties and meteorology) are specific to those sites. Using the limited measurement data for extrapolating the flux estimate in a large geographical area may not representative. In addition, most of these models treat vegetation as a net evasion source of Hg^0, which is inconsistent with later assessments that suggest vegetation a net sink (Gustin et al., 2008;Hartman et al., 2009). Recent isotopic tracer studies showed that that plant roots serve as a barrier that prevents translocation of inorganic Hg in soil to other parts of plants (Cui et al., 2014). It has also been suggested that Hg absorbed on foliage can be transported to stem and root (Yin et al., 2013). In addition, algorithms representing the transport resistances at soil and foliage interfaces were developed to calculate the multilayered, bidirectional flux through a Hg concentration gradient between ambient level and a "compensation" point inferred from the surface characteristics (Bash, 2010;Bash et al., 2007;Scholtz et al., 2003;Zhang et al., 2009a;Sutton et al., 2007). This approach is more scientifically sound and mathematically robust. The model results also seem to be more consistent with those from stable isotope studies (Bash, 2010). However, the complicated model parameterization makes it difficult to understand the relative importance of model variables on the simulated flux. It also requires assumptions for numerous model variables that lack field data to estimate their values. Although the model results can be constrained by air concentration and wet deposition, the assumptions could increase the uncertainty of model estimates and limits the improvement of model algorithms.

The objectives of this study are to present an updated Hg^0 air-surface exchange model and to quantitatively examine the relative importance of the physical and environmental variables implemented

in the model. Coupled with the latest understanding in the partitioning and mass transfer at different atmosphere-biosphere interfaces, we integrated the bidirectional air-surface exchange model (Bash, 2010;Bash et al., 2007) and the surface resistance schemes of Hg dry deposition and photochemical reaction (Zhang et al., 2003;Zhang et al., 2009a;Lin et al., 2006) for quantifying the air-surface exchange of Hg^0. Two monthly simulations were performed to investigate the seasonal and diurnal variability of the model-estimated flux. A systematic set of sensitivity simulations using multi-step factorial designs of experiments were performed to investigate the effect of significant model parameters and their interconnections. Based on the sensitivity results, processes that control Hg^0 air-surface exchange over different natural surfaces are discussed and research needs for future model improvement are proposed.

2 Methods

2.1 Model Description

The total air-surface exchange is the sum of Hg^0 fluxes from water, soil (including bare lands and soil under the canopy) and foliage surfaces. The direction (evasion or deposition) of the flux is driven by the gradient between atmospheric Hg^0 concentration and a surface compensation point that represents the Hg^0 concentration at the interface between the atmosphere and a natural surface. The magnitude of the flux is determined by the ratio of concentration gradient to surface resistance (for terrestrial surfaces) or by the product of overall mass transfer coefficient and concentration gradient (for water surfaces). The nomenclature and dimension of the entire set of model variables are detailed in Table 1. The parameterization of each model component is briefly described below.

2.2 Air-water Exchange

The flux over fresh water and oceanic surfaces, F_w, is calculated using a two-film mass transfer model with the transfer rate limited by the diffusion in the water boundary layer (Poissant et al., 2000):

$$F_w = K_w(C_w - \frac{C_{atm}}{H_w}) \quad (1)$$

where K_w is the overall mass transfer coefficient estimated by the wind speed at 10 m above water surface and the mass transfer ratio of CO_2/Hg across the air-water interface (Shetty et al., 2008), C_w is the DGM concentration in surface water, H_w is the dimensionless Henry's law constant. K_w and H_w are calculated using formulation described earlier (Poissant et al., 2000;Lin and Tao, 2003).

2.3 Air-terrestrial Exchange

The terrestrial system is divided into two categories: the canopy biomes (leaf area index, LAI > 0) and the bare lands (LAI = 0, referring to barren or sparsely vegetated land, bare ground tundra and snow or ice surface). The total flux from the canopy is made up of the air-soil exchange flux and the air-foliar exchange flux (air-stomata and air-cuticle). Over the canopy system, a multi-layer canopy resistance scheme modified after Bash (2010) and Zhang et al. (2003) was applied (Figure 1). Compared to the earlier mechanistic schemes, this model also (1) includes foliage storage effect is included, (2) considers photochemical reduction on foliage, and (3) updates the resistance terms. The flux over canopy biomes, F_{cnp}, is estimated as:

$$F_{cnp} = \frac{\Delta t}{(R_a+R_b)}(\chi_{cnp} - C_{atm}) \quad (2)$$

where Δt is time duration, R_a is the aerodynamic resistance, R_b is the quasi-laminar sub-layer resistance, C_{atm} is the atmospheric Hg concentration. R_a and R_b are calculated according to (Marsik et al., 2007). χ_{cnp} is the overall compensation point parameterized as a weighted average of exchange coefficients at the air-cuticle, air-stomata, and air-soil interfaces as illustrated in Figure 1 (Bash, 2010;Zhang et al., 2009a):

$$\chi_{cnp} = \frac{\frac{\chi_c}{R_c}+\frac{\chi_s}{R_s}+\frac{\chi_g}{R_g+R_{ac}}+\frac{C_{atm}}{R_a+R_b}}{\frac{1}{R_c}+\frac{1}{R_s}+\frac{1}{R_g+R_{ac}}+\frac{1}{R_a+R_b}} \quad (3)$$

whereχ_c is the cuticular compensation point, χ_s is the stomatal compensation point, χ_g is the soil compensation point, R_c is the cuticular resistance, R_s is the stomatal resistance, R_g is the soil diffusion resistance, R_{ac} is the in-canopy aerodynamic resistance. The individual compensation points are described by Equations 6, 9 and 15.

2.3.1 Air-soil Exchange

In absence of vegetation (when *LAI*=0), the flux from bare lands (F_{bls}) can be estimated as:

$$F_{bls} = \frac{\Delta t}{R_a+R_b+R_g}\left(\chi_g - C_{atm}\right) \quad (4)$$

In the presence of vegetation (when LAI > 0), the flux from soil under canopy (F_g) is calculated as:

$$F_g = \frac{\Delta t}{R_g+R_{ac}}\left(\chi_g - \chi_{cnp}\right) \quad (5)$$

where R_{ac} accounts for the resistance of gas diffusion from ground to the lower canopy and is assumed to be common for all gaseous species (Zhang et al., 2002b).The compensation point at air-soil interface (χ_g) can be expressed as (Bash, 2010):

$$\chi_g = \frac{[Hg^0]_{sl}H}{f_{oc}K_{oc}} \quad (6)$$

where $[Hg^0]_{sl}$ is the concentration of Hg^0 bound to soil, calculated as a reduction product of Hg(II) using soil Hg content and a pseudo-first-order rate constant related to solar irradiance (Gustin et al., 2002). *H* is Henry's constant parameterized following Andersson et al. (2008). f_{oc} is the fraction of organic carbon in surface soil (0-5 cm). K_{oc} is the partition coefficient of Hg^0 between soil organic carbon and water. R_g is the Hg^0 diffusion resistance over a ground surface (soil, ice/snow) (Zhang et al., 2002b):

$$\frac{1}{R_g} = \frac{\alpha_{Hg^0}}{R_{g(SO_2)}} + \frac{\beta_{Hg^0}}{R_{g(O_3)}} \quad (7)$$

where $R_{g(SO_2)}$ and $R_{g(O_3)}$ are the diffusion resistances of SO_2 and O_3, α_{Hg^0} is the Hg^0 scaling factor based on SO_2, β_{Hg^0} is Hg^0 scaling factor based on O_3. The formulation of $R_{g(SO_2)}$ and $R_{g(O_3)}$ has been described previously (Zhang et al., 2003).

142

143 2.3.2 Air-cuticle Exchange

144 Air -cuticle exchange flux is calculated as (Bash, 2010):

145 $$F_c = \frac{\Delta t}{R_c}(\chi_c - \chi_{cnp}) \quad (8)$$

146 $$\chi_c = \frac{[Hg_c^0]}{LAP} \quad (9)$$

147 where LAP denotes the leaf-air partitioning coefficient for Hg^0 (Rutter et al., 2011), $[Hg_c^0]$ is the
148 concentration of Hg^0 bound to foliar cuticular surface, calculated as the photoreduction product of a
149 fraction of newly deposited Hg(II) on foliar interfaces (Graydon et al., 2009):

150 $$[Hg_c^0] = f_{rxn}[Hg_{c,DD}^{II+}] \quad (10)$$

151 $$[Hg_c^{II+}] = (1 - f_{rxn} - f_{fixed})[Hg_{c,DD}^{II+}] \quad (11)$$

152 $$[Hg_c^{II+}] = \frac{[Hg_w^{II+}]}{T_l} \quad (12)$$

153 where $[Hg_{c,DD}^{II+}]$ is the concentration loading of total dry deposited Hg(II) on cuticle, $[Hg_c^{II+}]$ is the
154 concentration of the deposited Hg(II) residing on cuticular surfaces, $[Hg_w^{II+}]$ is the concentration of Hg(II)
155 that can be washed off from leaves, f_{rxn} is the fraction of Hg(II) that can be photo-reduced, f_{fixed} is the
156 fraction of Hg(II) fixed into tissue and not available for re-emission or wash-off, T_l is the leaf thickness.
157 f_{rxn}, f_{fixed} are parameterized following Smith-Downey et al. (2010). R_c is the cuticular resistance
158 calculated as (Zhang et al., 2002b):

159 $$\frac{1}{R_c} = \frac{\alpha_{Hg^0}}{R_{c(SO_2)}} + \frac{\beta_{Hg^0}}{R_{c(O_3)}} \quad (13)$$

160

161 2.2.3 Air-stomata Exchange

162 The air-stomata exchange flux is estimated as (Bash, 2010):

163 $$F_s = \frac{\Delta t}{R_s}(\chi_s - \chi_{cnp}) \quad (14)$$

$$\chi_S = \frac{[Hg_S^0]}{LAP} \quad (15)$$

It is assumed that the uptake of Hg species through stomata is predominantly Hg^0 due to its abundance in the atmosphere (Capiomont et al., 2000;Millhollen et al., 2006;Stamenkovic and Gustin, 2009). As such, the dissolved Hg^0 in the stomatal compartment, $[Hg_S^0]$, can be formulated as:

$$[Hg_S^0] = (1 - f_{fixed})[Hg_{S,DD}^0] \quad (16)$$

where $[Hg_{S,DD}^0]$ is the concentration of newly deposited Hg^0 stored in the stomatal compartment. The overall stomatal resistance is calculated as (Zhang et al., 2002b):

$$R_S = \frac{R_{st}+R_{me}}{1-W_{st}} \quad (17)$$

where R_{st} is the resistance associated with stomata, R_{me} is resistance associated with mesophyll reservoir, W_{st} is the fraction of stomatal blocking under wet condition. The detailed formulation of R_{st} and R_{me} and W_{st} can be found elsewhere (Zhang et al., 2012;Zhang et al., 2003;Zhang et al., 2002b).

2.4 Modeling Experiments for Sensitivity Analysis

A series of 2-level factorial designs of experiments were performed to assess the sensitivity to changes of model variables as well as their synergistic and antagonistic interactions. A brief discussion of the use of factorial design of experiments is provided in the Supplementary Material document. The studied variables include both physical and environmental parameters. Their respective experimental levels are show in Tables 2-4. The principle of factor sparsity (Myers et al., 2009) states that the main effects and lower-order interactions dominate most system responses and the higher-order interactions are not significant. Therefore, the effect of interaction terms higher than second order was not considered.

For water surface, there are four factors driving the model simulation (Table 2). Therefore, a 2^4 full factorial design was applied. For bare lands, the 11 model parameters (Table 3) form a 2^{11-6} fractional

187 design (Resolution IV) enabling main effects free from aliasing. The number of runs (32), although
188 intensive, is still manageable. After this initial screening, a two-level full factorial design was applied for
189 the significant factors based on a 95% confidence level (results of the 2^{11-6} design are shown in
190 Supplementary Material). For the canopy ecosystem, 15 main factors (Table 4) were selected to form a
191 2^{15-9} fractional design (Resolution IV, 64 experiments). In this case, the alias system is more complex
192 because of the large number of study factors. Therefore, a successive $2^{(11-6)}$ design (Supplementary
193 Material) was applied to the pre-screened significant factors to obtain 5 most significant factors for a 2^5
194 full factorial design (Supplementary Material). The sensitivity results were illustrated based on the final
195 full factorial design for watersheds, bare lands, canopy ecosystems. The data analysis of the factorial
196 experiments was conducted using Minitab®16.
197
198 2.5 Model Configuration and Data
199 The modeling domain is in Lambert Conformal projection covering mainly the Contiguous United States
200 (CONUS), with 156×118 grid cells at 36-km spatial resolution. Hourly meteorological data were prepared
201 using the Weather Research and Forecasting (WRF) model Version 3.4 with the Noah Land Surface
202 Model. The model algorithms were coded in FORTRAN 90 and Network Common Data Form (NetCDF)
203 version 4.1. The gridded model results were visualized by the Visualization Environmental for Rich Data
204 Interpretation (VERDI) version 1.4.
205
206 A base-case simulation was performed in a summer and a winter month (August & December 2009) to
207 evaluate the seasonal and diurnal variability of the air-surface exchange. The base case refers to the
208 modeling utilizing the values listed in Table 1 with the meteorological parameters extracted from WRF
209 output. In the simulation, the atmospheric Hg^0 concentration retrieved from the output of the Hg
210 extension of Community Multi-scale Air Quality modeling system (CMAQ-Hg) version 4.6 for the same

211 modeling period was applied to represent the air concentration of Hg^0. The simulation does not directly
212 incorporate the feedback of the air-surface exchange to the air concentration. However, for a regional
213 model domain (CONUS), natural evasion and deposition of Hg^0 does not significantly modify the
214 ambient concentration (Lin et al., 2005; Gbor et al., 2006), since the time required for air turnover is
215 relatively short (typically 3-4 days) and the air concentration of Hg is mainly controlled by the boundary
216 conditions (Pongprueksa et al., 2008). In the model experiments, the concentration of Hg^0 was tested as a
217 sensitivity parameter.
218

219 **3 Results and Discussion**

220 3.1 Results of Base-case Simulations

221 The model estimates a net emission of 38.4 Mg in the summer month (16.6 Mg from water, 45.0 Mg from
222 soil and -23.2 Mg from foliage) and 56.0 Mg in the winter month (33.9 Mg from water, 29.5 Mg from soil
223 and -7.4 Mg from foliage) for the entire domain. The evasion from water body accounts for ~50% of the
224 total natural emission (the cumulative net release of Hg^0 caused by the air-surface exchange process)
225 because of the large water areal coverage in the domain (59%). Vegetation represents a net sink, this is
226 different from earlier estimates using the evapotranspiration approach (Bash et al., 2004;Shetty et al.,
227 2008) but consistent with recent observational studies (Gustin et al., 2008;Stamenkovic and Gustin, 2009).
228 For the terrestrial system, the total emission is 43.9 Mg in two months. Assuming the annual emission is
229 5-6 times of the two monthly sum and excluding the emission from Canada, Mexico and Caribbean lands,
230 the model-estimated annual emission in the contiguous US is 118-141 Mg yr^{-1}, comparable to the recent
231 estimates (95-150 Mg yr^{-1}) using flux scaling methods (Ericksen et al., 2006;Hartman et al., 2009;Zehner
232 and Gustin, 2002).
233

234 3.1.1 Air-water Exchange

Over water surface, the mean simulated flux is 1.6 and 3.1 ng m^{-2} hr^{-1} in the summer and winter month (Figures 2a&3a) respectively. Water bodies in the domain are net sources, producing fluxes typically in the range of 1-4 ng m^{-2} hr^{-1}, similar to earlier measurements (Mason et al., 2001a;Andersson et al., 2011). The spatial distribution is primarily driven by the surface wind speed. Temperature, air Hg^0 and DGM concentration play a much less significant role because a constant DGM was assumed (40 ng m^{-3}) and the Hg^0 level over water was in a narrow range (1.4 ~1.8 ng m^{-3}). The Pearsons's correlation coefficient (r) between flux and wind speed is much stronger than the value between flux and temperature (0.56 vs. 0.18). The flux in the winter month is greater because of stronger winds in the northeastern corner of the domain. The emission flux does not show clear diurnal variation in both months because wind speed is the most dominant factor (Figure 4a).

3.1.2 Air-soil Exchange

Soil surfaces have been suggested to be a net source of Hg (Gustin et al., 2008;Hartman et al., 2009), which is also shown in the base-case model results (Figure 2&3). The mean flux from bare lands (0.7 and 0.6 ng m^{-2} hr^{-1} in the summer and winter month) is lower than the value from soil under the canopy (4.3 and 2.7 ng m^{-2} hr^{-1}) because of the landuse classification. The bare lands in the domain include sparsely vegetated land, bare ground tundra and snow/ice land. The flux contribution from such landuse types is largely from the southern portion of the domain. The simulated flux from soil under canopy is comparable to those reported at background sites, -0.1~7 ng m^{-2} hr^{-1} (Ericksen et al., 2006;Kuiken et al., 2008b;Kuiken et al., 2008a;Carpi and Lindberg, 1998).

The simulated Hg^0 flux from soil under canopy is controlled by the degree of vegetation coverage (LAI), air temperature, friction velocity, air Hg concentration and solar irradiation. In the summer month, the flux in Eastern US is lower due to heavy vegetation coverage that increases the in-canopy aerodynamic

resistance (R_{ac}) (Zhang et al., 2002a). Higher flux occurs in the Central and Western US because of the smaller LAI and higher air temperature (Figure 2c， Figure s8). In the winter month, the higher air temperature and longer sunlit hours cause the higher flux in the south (Figure 3c, Figure s8). Among the environmental parameters, LAI has the greatest influence on the estimated flux (r = 0.45). The spatially average soil flux for the entire domain shows a typical diurnal variation caused by air temperature and solar irradiance (Gabriel et al., 2006). The detailed impact of the model variables is discussed in the sensitivity analysis.

3.1.3 Air-foliage Exchange

Vegetation represents a net sink of Hg^0 in the base-case simulations. The mean simulated air-foliar exchange is -2.2 and -0.7 ng m^{-2} hr^{-1} in the summer and winter month (Figures 2d, 3d). The magnitude is similar to those measured in August by Ericksen et al. (2003) (a mean flux of -3.3 ng m^{-2} hr^{-1}) and Millhollen et al. (2006) (-4.1~-0.3 ng m^{-2} hr^{-1}). In summer, the greatest vegetative uptake of Hg^0 occurs in the Northeast US because of the dense vegetation coverage. In winter, the uptake becomes much weaker due to the reduced LAI, particularly in the north (Smith-Downey et al., 2010). The simulated deposition flux is highly correlated with LAI (r = 0.71 and 0.88 in winter and summer); while the correlations with friction velocity, GEM, air temperature and solar radiation are comparatively weaker. The diurnal variation for foliar flux is shown in Figure 4c. Higher deposition occurs during daytime due to the higher air temperature and solar irradiance (Rutter et al., 2011). The overall diurnal variation in the model domain exhibits the feature of air-foliage exchange (Figure 4d).

The simulated flux from soil under canopy and foliar surfaces is highly dependent on the resistance terms. Presently the values of cuticular (R_c), stomatal (R_g) and soil (R_s) resistances of Hg are not well understood (Holmes et al., 2011) and have been estimated by relating to the measured resistance of O_3, SO_2 and H_2O

283 (Bash, 2010;Scholtz et al., 2003;Zhang et al., 2003). There has been experimental efforts to determine R_c
284 and R_s based on Fick's Law by introducing isotopic Hg tracer to plants grown in an environmentally
285 controlled chamber (Rutter et al., 2011). The resistances were found to depend on temperature, solar
286 irradiance and Hg species with reported R_c and R_s ranging from 150 to 50000 m s^{-1} at 0-35°C and 0-170
287 W m^{-2} (Millhollen et al., 2006;Rutter et al., 2011). The simulated flux in the base case applied similar
288 resistance values in the model. However, the lack of deterministic relationships between the resistance
289 terms and environmental parameters still represents an uncertainty and there is a need to better quantify
290 the resistance for Hg^0.
291
292 **3.2 Sensitivities Analysis**
293 3.2.1 Sensitivity of Exchanges over Water Bodies
294 Figure 5 shows the change of air-water flux due to the change of model variables from the low to the high
295 experimental level (Table 2). Individually, wind speed is the most significant parameter (p = 0.003)
296 followed by DGM (p = 0.004) and surface temperature (p = 0.059). On average, increasing wind speed
297 from 0.001 to 20 m s^{-1} enhanced the flux by 7.6 ng m^{-2} hr^{-1} (p = 0.003); increasing the DGM from 15 to
298 240 ng m^{-3} increases the flux by 7.0 ng m^{-2} hr^{-1} (p = 0.004). A higher air Hg^0 concentration slightly
299 decreases the evasion flux. There is a significant synergistic effect caused by wind speed and DGM
300 concentration (p = 0.004). Increasing both variables simultaneously from the low to high level (Table 2)
301 causes an additional 48% increase of the evasion flux. The wind speed and surface temperature also have
302 a synergistic effect, although not as significant (p = 0.059), followed by the effect enhanced by DGM
303 concentration and surface temperature (p = 0.076). The effects of higher DGM concentration and air Hg^0
304 concentration offset each other, leading to a nearly zero effect on flux (p = 1.000).
305
306 In the base case, a uniform DGM concentration was assumed. The spatially constant DGM level

307 represents a significant uncertainty since other environmental parameters such temperature, wind speed
308 can be estimated reliably through meteorological simulations at a high spatial resolution. The mechanism
309 leading to the net DGM formation in surface water is complex and not fully understood (Qureshi et al.,
310 2010). It has been suggested that dissolved organic matter (Amyot et al., 1994;Amyot et al., 1997),
311 hydroxyl radicals (Zhang and Lindberg, 2001) and oxyhalide radicals (e.g. OCl^-, OBr^-) (Lalonde et al.,
312 2001) can participate in the sunlight-induced processes that produce DGM, in addition, DGM is also
313 consumed by some oxidation reactions in water bodies. Data on measured net DGM concentration over
314 vast water bodies are not readily available because of a limited number of cruise campaigns (Mason et al.,
315 1998;Mason et al., 2001b;Andersson et al., 2011). Strode et al. (2007) and Soerensen et al. (2010)
316 estimated the global distribution of DGM in sea water and showed that accurate representation of GDM
317 concentration is key for calculating air-water exchange. More knowledge on the temporal and spatial
318 distribution of net DGM concentration in surface water can greatly reduce the model uncertainty.
319 Experimental investigation to better understand the chemical pathways leading to net DGM formation
320 will also help constrain the model estimate.
321
322 3.2.2 Sensitivity of Exchange over Bare Lands
323 Figure 6 illustrates the model response to the model variables at the two experimental levels in Table 3.
324 Soil Hg content, friction velocity, air temperature and the scaling factor β_{Hg^0} (Eq. 7) have a positive
325 effect on the simulated Hg flux while the soil organic content has a negative effect. On average,
326 increasing soil Hg content from 50 to 1000 ng g^{-1} soil enhances the flux by 55.3 ng m^{-2} hr^{-1} (p = 0.013);
327 increasing friction velocity from 0.0001 to 1 m s^{-1} increases the flux by 54.8 ng m^{-2} hr^{-1} (p = 0.014). On
328 the other hand, increasing the soil organic content from 0.6 to 10 % reduce the flux by 54.2 ng m^{-2} hr^{-1} (p
329 = 0.015). There are several notable interactions among the model variables. First, the positive effects of
330 soil Hg content and friction velocity can be completely offset by soil organic content (Figure 6). An

increase in soil organic content substantially decreases the soil Hg compensation point (Eq. 6), suggesting the significant role of soil organic matter in retaining Hg from evading (p = 0.025). There is a strong synergistic effect between friction velocity and soil Hg content (p = 0.022), leading to an additional 46% increase compared to the sum of the two individual effects (Figure 6). Quasi-laminar sub-layer resistance (R_b) and aerodynamic resistance (R_a) both decrease with increasing friction velocity. Coupled with the increased soil Hg compensation point at higher soil Hg content (Eq. 6), the flux is greatly enhanced (Figure 6). Overall, that friction velocity, soil Hg and organic content are the most influential parameters for Hg exchanges over bare lands. Other pre-screened parameters including temperature, Hg scaling factor (β_{Hg} in Eq. 7) and other interaction terms have less significant impact.

3.2.3. Sensitivity of Exchange over Canopy

Figure 7 illustrates the sensitivity of simulated Hg flux over canopy to the model variables at the two experimental levels in Table 4. For comparison, the sensitivity results for air-soil exchange under canopy are also shown. It is clear that the forcing of air-canopy exchange is dominated by the air-soil exchange under canopy at the two experimental levels. This resembles the Hg^0 emission characteristics observed in a gas exchange system, which suggested that the evasion from soils is much greater than the emission from the plants grown in the chamber (Frescholtz and Gustin, 2004;Frescholtz et al., 2003). After the factor pre-screening step (Figures s2-s7 in Supplementary Material), the simulated flux is particularly sensitive to the change of five parameters. Friction velocity (positive effect, p = 0.020), soil Hg content (positive effect, p = 0.028) and soil organic content (negative effect, p = 0.030) are the most significant model parameters (Figure 7). These effects are similar to the sensitivity results of air-soil exchange over bare lands (Figures 6 & 7), but slightly weaker based on the p values because of the "shielding" of vegetation coverage that modifies the values of the resistance terms (R_b and R_{ac}) (Zhang et al., 2002a). Highly moist soil (soil moisture content > 20%, Table 4) has a negative effect because it effectively

355 increases soil diffusion resistance (R_g) (Zhang et al., 2003), although the effect is less significant (p =
356 0.289). Air temperature also has a positive effect as anticipated (p = 0.180).
357
358 The synergistic effect caused by friction velocity and soil Hg content is significant for the air-canopy
359 exchange (p = 0.028, Figure 7), enhancing the evasion flux by 47 % (77.8 ng m^{-2} hr^{-1}). Both soil organic
360 content and highly moist soil condition can offset the positive effects caused by higher friction velocity,
361 soil Hg content and air temperature at different degrees (Figure 7), with the soil organic content being
362 more influential. Higher soil organic content at high soil moisture (>20 %) yields a weak positive effect
363 (p = 0.340), this is interpreted as the combined negative effect of the two parameters is smaller than the
364 sum of the two individual effects. Overall, these characteristics resemble the air-soil exchange because the
365 air-canopy exchange is dominated by the air-soil exchange under canopy.
366
367 Atmospheric mercury can deposit on the surface of cuticle or be accumulated in leaves through stomatal
368 uptake (Figure 1). For cuticular exchange, air temperature has a significant positive effect (Figure 8).
369 Since air-cuticle exchange is mainly deposition (negative flux), this means that a higher air temperature
370 leads to smaller deposition or greater evasion (p < 0.001). Friction velocity has a strong negative effect
371 (i.e., higher deposition at higher friction velocity, p < 0.001) on the simulated flux. Higher soil organic
372 content (p = 0.009) and highly moist (>20%) soil (p = 0.194) increase the simulated flux (i.e., weaken the
373 deposition) by decreasing the canopy compensation point (χ_c in Eq. 8). Under the circumstance, Hg
374 deposits preferentially to soil and therefore a reduced deposition on cuticle. Higher soil Hg content
375 decreases the flux (p = 0.008) by increasing the overall compensation point (χ_{cnp} in Eq. 8), suggesting
376 greater deposition on cuticle at higher soil Hg content. For stomatal exchange, the trend of single factor
377 effect is the same as that of cuticular exchange.
378

379 Several notable interaction effects are observed for foliar exchanges. For cuticle exchange, the deposition
380 is reversed from deposition to evasion at the high air temperature level, leading to the overall positive
381 interaction effect for air temperature and friction velocity (Figure 8, $p < 0.001$). The positive effect of soil
382 organic content significantly offsets the negative effect of friction velocity ($p = 0.010$) and soil Hg content
383 ($p = 0.016$). For stomatal exchange, the only significant interaction effect is between soil organic and Hg
384 content, which is more dominated by soil organic content. Overall, the foliar exchange is primarily
385 controlled by air temperature and friction velocity because the resistance terms can be affected by the two
386 variables. This is in contrast to the evapotranspiration approach where soil Hg content plays a
387 predominant role in simulated Hg^0 evasion flux (Bash et al., 2004;Gbor et al., 2006).
388
389 In this analysis, the effect of solar irradiance is *not* as significant as the selected parameters under the
390 resistance model scheme and has been ruled out during the pre-screening for the model variables (Section
391 2.4 and Figures s2~s6). In the model, solar irradiation can influence the flux in three ways: (1) through
392 modifying the rate constant of Hg(II) reduction in soils and foliage (Eqs. 6 &10 &16), (2) through forcing
393 the change of aerodynamic resistance (R_a and R_{ac}), and (3) through forcing the change of cuticular and
394 stomatal resistance terms (R_c and R_{st}). For air-soil exchange, the effect of solar irradiance on the reduction
395 rate constant is the most sensitive process (Eqs. 6 & 10). The photoreduction of Hg(II) in soils has been
396 suggested to be responsible for the increased soil flux observed under sunlit condition (Gustin et al.,
397 2002). There have been kinetic studies showing that increasing UV-A intensity by 75% approximately
398 doubles the photoreduction rate in the aqueous phase (Qureshi et al., 2010). However, the effect of lights
399 on the kinetics of Hg(II) reduction in soils is poorly understood. In this modeling, the photoreduction rate
400 constant was set to a mean value (Eq. 6). This limits a full examination of the true impact of solar
401 irradiation on the simulated Hg flux. Results from experimental studies on Hg(II) photoreduction rates
402 will help reduce this model uncertainty. For foliar exchange, solar irradiation has a weak positive effect

403 on the flux (i.e., slightly weakens deposition, Figure s4), but has a significant positive effect on the
404 stomatal exchange (p= 0.004, Figure s5).
405
406 **4 Conclusions**
407 An updated model for estimating the bidirectional air-surface exchange of Hg is presented based on the
408 current understanding of surface resistance schemes. From the base-case results, water and soil surfaces
409 are net sources and vegetation is a net sink of Hg^0. Each natural surface exhibits a different diurnal and
410 seasonal variation. Sensitivity analysis of model variables using a 2-level factorial design of experiments
411 shows that atmospheric shear flows (surface wind over water and friction velocity of terrestrial surfaces),
412 dissolved gaseous mercury (DGM) concentration, soil organic and Hg content, and air temperature are the
413 most influential factors controlling the magnitude of the atmosphere-biosphere exchange of Hg^0.
414 However, the positive effect of friction velocity and soil Hg content on the evasion flux from soil and
415 canopy can be greatly offset by the negative effect of soil organic content. Significant synergistic effects
416 are identified between surface wind and DGM level for water surface, and between soil Hg content and
417 friction velocity for soil surface, leading to ~50% enhanced flux in the combined effect compared to the
418 sum of their individual effects. The air-foliar exchange is mainly controlled by surface resistance terms
419 controlled by environmental parameters such as solar irradiation and air temperature.
420
421 The uncertainty in this modeling assessment is primarily from the lack of knowledge in (1) the spatial
422 distribution of organic and Hg content in soil and DGM concentration in water, (2) the reduction
423 mechanism and kinetics of Hg(II) in soil and water, and (3) the values of resistance terms over different
424 natural surfaces. More research in providing geospatial distribution of Hg in water and soil will greatly
425 improve the model estimate. Further elucidation on the interaction of Hg and organic carbon in top soil
426 and surface water as well as quantification of the surface resistance terms specific to Hg species will also

help improve the model scheme. Recent field and experimental investigations have suggested that organic carbon in soil potentially shapes the distribution of Hg in forest at continental scales (Obrist et al., 2011) and that the long-term Hg evasion from soil is highly related to the Hg and organic carbon interactions (Smith-Downey et al., 2010). Given the predominance of soil organic content in reducing soil Hg evasion flux using the mechanistic approach in this study, soil organic content is likely the controlling factor determining the intensity of air-soil Hg^0 exchange.

Acknowledgements

This work was funded by National "973" Program of China (2013CB430003), National Institute of Food and Agriculture, U.S. Department of Agriculture (2009-38899-20017), and State Key Laboratory of Environmental Geochemistry, IGCAS. The funding support is gratefully acknowledged. We thank Pruek Pongprueksa for providing Hg concentration/deposition data for this work and Pattaraporn Singhasuk for creating the visualization in Figure 1.

References

Akkarappuram, A. F., and Raman, S.: A comparison of surface friction velocities estimated by dissipation and iterative bulk aerodynamic methods during gale, Geophys. Res. Lett., 15, 401-404, 10.1029/GL015i005p00401, 1988.

Amyot, M., Mierle, G., Lean, D. R. S., and Mcqueen, D. J.: Sunlight-Induced Formation of Dissolved Gaseous Mercury in Lake Waters, Environmental Science & Technology, 28, 2366-2371, Doi 10.1021/Es00062a022, 1994.

Amyot, M., Gill, G. A., and Morel, F. M. M.: Production and loss of dissolved gaseous mercury in coastal seawater, Environmental Science & Technology, 31, 3606-3611, Doi 10.1021/Es9703685, 1997.

Andersson, M. E., Gardfeldt, K., Wangberg, I., and Stromberg, D.: Determination of Henry's law constant for elemental mercury, Chemosphere, 73, 587-592, DOI 10.1016/j.chemosphere.2008.05.067, 2008.

Andersson, M. E., Sommar, J., Gardfeldt, K., and Jutterstrom, S.: Air-sea exchange of volatile mercury in the North Atlantic Ocean, Marine Chemistry, 125, 10.1016/j.marchem.2011.01.005, 2011.

454 Bash, J. O., Miller, D. R., Meyer, T. H., and Bresnahan, P. A.: Northeast United States and Southeast
455 Canada natural mercury emissions estimated with a surface emission model, Atmospheric
456 Environment, 38, 5683-5692, 10.1016/j.atmosenv.2004.05.058, 2004.
457 Bash, J. O., Bresnahan, P., and Miller, D. R.: Dynamic surface interface exchanges of mercury: A review
458 and compartmentalized modeling framework, Journal of Applied Meteorology and Climatology, 46,
459 1606-1618, 10.1175/jam2553.1, 2007.
460 Bash, J. O.: Description and initial simulation of a dynamic bidirectional air-surface exchange model for
461 mercury in Community Multiscale Air Quality (CMAQ) model, Journal of Geophysical Research-
462 Atmospheres, 115, D0630510.1029/2009jd012834, 2010.
463 Calhoun, F. G., Smeck, N. E., Slater, B. L., Bigham, J. M., and Hall, G. F.: Predicting bulk density of Ohio
464 soils from morphology, genetic principles, and laboratory characterization data, Soil Sci Soc Am J,
465 65, 811-819, 2001.
466 Capiomont, A., Piazzi, L., and Pergent, G.: Seasonal variations of total mercury in foliar tissues of
467 Posidonia oceanica, J Mar Biol Assoc Uk, 80, 1119-1123, Doi 10.1017/S0025315400003192, 2000.
468 Carpi, A., and Lindberg, S. E.: Application of a Teflon (TM) dynamic flux chamber for quantifying soil
469 mercury flux: Tests and results over background soil, Atmospheric Environment, 32, 873-882, Doi
470 10.1016/S1352-2310(97)00133-7, 1998.
471 Cui, L. W., Feng, X. B., Lin, C. J., Wang, X. M., Meng, B., Wang, X., and Wang, H.: ACCUMULATION AND
472 TRANSLOCATION OF (198)HG IN FOUR CROP SPECIES, Environmental Toxicology and Chemistry, 33,
473 334-340, 10.1002/etc.2443, 2014.
474 Ericksen, J. A., Gustin, M. S., Schorran, D. E., Johnson, D. W., Lindberg, S. E., and Coleman, J. S.:
475 Accumulation of atmospheric mercury in forest foliage, Atmospheric Environment, 37,
476 10.1016/s1352-2310(03)00008-6, 2003.
477 Ericksen, J. A., Gustin, M. S., Xin, M., Weisberg, P. J., and Fernandez, G. C. J.: Air-soil exchange of mercury
478 from background soils in the United States, Science of the Total Environment, 366,
479 10.1016/j.scitotenv.2005.08.019, 2006.
480 Fay, L., and Gustin, M.: Assessing the influence of different atmospheric and soil mercury concentrations
481 on foliar mercury concentrations in a controlled environment, Water Air and Soil Pollution, 181,
482 373-384, DOI 10.1007/s11270-006-9308-6, 2007.
483 Frescholtz, T. F., Gustin, M. S., Schorran, D. E., and Fernandez, G. C. J.: Assessing the source of mercury in
484 foliar tissue of quaking aspen, Environmental Toxicology and Chemistry, 22, 2114-2119, Doi
485 10.1897/1551-5028(2003)022<2114:Atsomi>2.0.Co;2, 2003.
486 Frescholtz, T. F., and Gustin, M. S.: Soil and foliar mercury emission as a function of soil concentration,
487 Water Air and Soil Pollution, 155, 223-237, Doi 10.1023/B:Wate.0000026530.85954.3f, 2004.

Friedli, H. R., Arellano, A. F., Cinnirella, S., and Pirrone, N.: Initial Estimates of Mercury Emissions to the Atmosphere from Global Biomass Burning, Environmental Science & Technology, 43, 3507-3513, Doi 10.1021/Es802703g, 2009.

Gabriel, M. C., Williamson, D. G., Zhang, H., Brooks, S., and Lindberg, S.: Diurnal and seasonal trends in total gaseous mercury flux from three urban ground surfaces, Atmospheric Environment, 40, 10.1016/j.atmosenv.2006.04.004, 2006.

Gbor, P. K., Wen, D. Y., Meng, F., Yang, F. Q., Zhang, B. N., and Sloan, J. J.: Improved model for mercury emission, transport and deposition, Atmospheric Environment, 40, 973-983, DOI 10.1016/j.atmosenv.2005.10.040, 2006.

Gower, S. T., Kucharik, C. J., and Norman, J. M.: Direct and indirect estimation of leaf area index, f(APAR), and net primary production of terrestrial ecosystems, Remote Sens Environ, 70, 29-51, Doi 10.1016/S0034-4257(99)00056-5, 1999.

Graydon, J. A., St Louis, V. L., Hintelmann, H., Lindberg, S. E., Sandilands, K. A., Rudd, J. W. M., Kelly, C. A., Tate, M. T., Krabbenhoft, D. P., and Lehnherr, I.: Investigation of Uptake and Retention of Atmospheric Hg(II) by Boreal Forest Plants Using Stable Hg Isotopes, Environmental Science & Technology, 43, 10.1021/es900357s, 2009.

Guo, Y. Y., Amundson, R., Gong, P., and Yu, Q.: Quantity and spatial variability of soil carbon in the conterminous United States, Soil Sci Soc Am J, 70, 590-600, DOI 10.2136/sssaj2005.0162, 2006.

Gustin, M. S., Biester, H., and Kim, C. S.: Investigation of the light-enhanced emission of mercury from naturally enriched substrates, Atmospheric Environment, 36, 3241-3254, Pii S1352-2310(02)00329-1Doi 10.1016/S1352-2310(02)00329-1, 2002.

Gustin, M. S., Lindberg, S. E., and Weisberg, P. J.: An update on the natural sources and sinks of atmospheric mercury, Applied Geochemistry, 23, 10.1016/j.apgeochem.2007.12.010, 2008.

Hartman, J. S., Weisberg, P. J., Pillai, R., Ericksen, J. A., Kuiken, T., Lindberg, S. E., Zhang, H., Rytuba, J. J., and Gustin, M. S.: Application of a Rule-Based Model to Estimate Mercury Exchange for Three Background Biomes in the Continental United States, Environmental Science & Technology, 43, 10.1021/es900075q, 2009.

Holmes, H. A., Pardyjak, E. R., Perry, K. D., and Abbott, M. L.: Gaseous dry deposition of atmospheric mercury: A comparison of two surface resistance models for deposition to semiarid vegetation, Journal of Geophysical Research-Atmospheres, 116, D14306 10.1029/2010jd015182, 2011.

Jones, R. J. S., Rusco, R. H. E., Loveland, P. J., and Montanarella, L.: The map of organic carbon in topsoils in Europe: Explanation of Special Publication Ispra 2004 No.72 (S.P.I.04.72)17, EUR 21209 EN, 2004.

Kuiken, T., Gustin, M., Zhang, H., Lindberg, S., and Sedinger, B.: Mercury emission from terrestrial background surfaces in the eastern USA. II: Air/surface exchange of mercury within forests from South Carolina to New England, Applied Geochemistry, 23, 10.1016/j.apgeochem.2007.12.007, 2008a.

524 Kuiken, T., Zhang, H., Gustin, M., and Lindberg, S.: Mercury emission from terrestrial background
525 surfaces in the eastern USA. Part I: Air/surface exchange of mercury within a southeastern
526 deciduous forest (Tennessee) over one year, Applied Geochemistry, 23,
527 10.1016/j.apgeocliem.2007.12.006, 2008b.
528 Kwun, J. H., and You, S. H.: Numerical Study of Sea Winds Simulated by the High-Resolution Weather
529 Research and Forecasting (WRF) Model, Asia-Pac J Atmos Sci, 45, 523-554, 2009.
530 Lalonde, J. D., Amyot, M., Kraepiel, A. M. L., and Morel, F. M. M.: Photooxidation of Hg(0) in artificial and
531 natural waters, Environmental Science & Technology, 35, 1367-1372, Doi 10.1021/Es001408z, 2001.
532 Lin, C. J., Lindberg, S. E., Ho, T. C., and Jang, C.: Development of a processor in BEIS3 for estimating
533 vegetative mercury emission in the continental United States, Atmos Environ, 39, 7529-7540,
534 10.1016/j.atmosenv.2005.04.044, 2005.
535 Lin, C. J., Pongprueksa, P., Lindberg, S. E., Pehkonen, S. O., Byun, D., and Jang, C.: Scientific uncertainties
536 in atmospheric mercury models I: Model science evaluation, Atmospheric Environment, 40, 2911-
537 2928, DOI 10.1016/j.atmosenv.2006.01.009, 2006.
538 Lin, X., and Tao, Y.: A numerical modelling study on regional mercury budget for eastern North America,
539 Atmospheric Chemistry and Physics, 3, 535-548, 2003.
540 Lindberg, S., Bullock, R., Ebinghaus, R., Engstrom, D., Feng, X., Fitzgerald, W., Pirrone, N., Prestbo, E., and
541 Seigneur, C.: A synthesis of progress and uncertainties in attributing the sources of mercury in
542 deposition, Ambio, 36, 19-32, 2007.
543 Marsik, F. J., Keeler, G. J., and Landis, M. S.: The dry-deposition of speciated mercury to the Florida
544 Everglades: Measurements and modeling, Atmospheric Environment, 41, 136-149, DOI
545 10.1016/j.atmosenv.2006.07.032, 2007.
546 Mason, R. P., Rolfhus, K. R., and Fitzgerald, W. F.: Mercury in the North Atlantic, Marine Chemistry, 61,
547 37-53, Doi 10.1016/S0304-4203(98)00006-1, 1998.
548 Mason, R. P., Lawson, N. M., and Sheu, G. R.: Mercury in the Atlantic Ocean: factors controlling air-sea
549 exchange of mercury and its distribution in the upper waters, Deep-Sea Res Pt Ii, 48, 2829-2853,
550 Doi 10.1016/S0967-0645(01)00020-0, 2001a.
551 Mason, R. P., Sheu, G. R., and Lawson, N. M.: Redox chemistry of mercury at the air-water interface and
552 its role in the global cycling of mercury., Abstr Pap Am Chem S, 222, U429-U429, 2001b.
553 Mason, R. P., and Sheu, G. R.: Role of the ocean in the global mercury cycle, Global Biogeochemical
554 Cycles, 16, Artn 1093 Doi 10.1029/2001gb001440, 2002.
555 Millhollen, A. G., Gustin, M. S., and Obrist, D.: Foliar mercury accumulation and exchange for three tree
556 species, Environmental Science & Technology, 40, 6001-6006, Doi 10.1021/Es0609194, 2006.
557 Morel, F. M. M., Kraepiel, A. M. L., and Amyot, M.: The chemical cycle and bioaccumulation of mercury,
558 Annu Rev Ecol Syst, 29, 543-566, DOI 10.1146/annurev.ecolsys.29.1.543, 1998.

559 Myers, R. H., Montgomery, D. C., and Anderson-Cook, C. M.: Response Surface Methodology: Process
560 and Product Optimization Using Designed Experiments, 3 ed., Wiley Series in Probability and
561 Statistics, John Wiley & Sons Inc., New York, 704 pp., 2009.
562 Obrist, D., Johnson, D. W., Lindberg, S. E., Luo, Y., Hararuk, O., Bracho, R., Battles, J. J., Dail, D. B.,
563 Edmonds, R. L., Monson, R. K., Ollinger, S. V., Pallardy, S. G., Pregitzer, K. S., and Todd, D. E.:
564 Mercury Distribution Across 14 US Forests. Part I: Spatial Patterns of Concentrations in Biomass,
565 Litter, and Soils, Environmental Science & Technology, 45, 3974-3981, Doi 10.1021/Es104384m,
566 2011.
567 Pacyna, E. G., Pacyna, J. M., Steenhuisen, F., and Wilson, S.: Global anthropogenic mercury emission
568 inventory for 2000, Atmospheric Environment, 40, 4048-4063, DOI
569 10.1016/j.atmosenv.2006.03.041, 2006.
570 Pacyna, J. M., Pacyna, E. G., Steenhuisen, F., and Wilson, S.: Mapping 1995 global anthropogenic
571 emissions of mercury, Atmospheric Environment, 37, S109-S117, Doi 10.1016/S1352-
572 2310(03)00239-4, 2003.
573 Pirrone, N., Cinnirella, S., Feng, X., Finkelman, R. B., Friedli, H. R., Leaner, J., Mason, R., Mukherjee, A. B.,
574 Stracher, G. B., Streets, D. G., and Telmer, K.: Global mercury emissions to the atmosphere from
575 anthropogenic and natural sources, Atmospheric Chemistry and Physics, 10, 5951-5964, DOI
576 10.5194/acp-10-5951-2010, 2010.
577 Poissant, L., Amyot, M., Pilote, M., and Lean, D.: Mercury water-air exchange over the Upper St.
578 Lawrence River and Lake Ontario, Environmental Science & Technology, 34, 3069-3078, Doi
579 10.1021/Es990719a, 2000.
580 Poissant, L., Pilote, M., Yumvihoze, E., and Lean, D.: Mercury concentrations and foliage/atmosphere
581 fluxes in a maple forest ecosystem in Quebec, Canada, Journal of Geophysical Research-
582 Atmospheres, 113, 10.1029/2007jd009510, 2008.
583 Pongprueksa, P., Lin, C. J., Lindberg, S. E., Jang, C., Braverman, T., Bullock, O. R., Ho, T. C., and Chu, H. W.:
584 Scientific uncertainties in atmospheric mercury models III: Boundary and initial conditions, model
585 grid resolution, and Hg(II) reduction mechanism, Atmospheric Environment, 42, 1828-1845, DOI
586 10.1016/j.atmosenv.2007.11.020, 2008.
587 Qureshi, A., O'Driscoll, N. J., MacLeod, M., Neuhold, Y. M., and Hungerbuhler, K.: Photoreactions of
588 Mercury in Surface Ocean Water: Gross Reaction Kinetics and Possible Pathways, Environmental
589 Science & Technology, 44, 644-649, Doi 10.1021/Es9012728, 2010.
590 Rutter, A. P., Schauer, J. J., Shafer, M. M., Creswell, J., Olson, M. R., Clary, A., Robinson, M., Parman, A.
591 M., and Katzman, T. L.: Climate Sensitivity of Gaseous Elemental Mercury Dry Deposition to Plants:
592 Impacts of Temperature, Light Intensity, and Plant Species, Environmental Science & Technology,
593 45, 10.1021/es102687b, 2011.

Scholtz, M. T., Van Heyst, B. J., and Schroeder, W.: Modelling of mercury emissions from background soils, Science of the Total Environment, 304, 185-207, 10.1016/s0048-9697(02)00568-5, 2003.

Selin, N. E., and Jacob, D. J.: Seasonal and spatial patterns of mercury wet deposition in the United States: Constraints on the contribution from North American anthropogenic sources, Atmospheric Environment, 42, 5193-5204, DOI 10.1016/j.atmosenv.2008.02.069, 2008.

Shetty, S. K., Lin, C. J., Streets, D. G., and Jang, C.: Model estimate of mercury emission from natural sources in East Asia, Atmospheric Environment, 42, 8674-8685, DOI 10.1016/j.atmosenv.2008.08.026, 2008.

Smith-Downey, N. V., Sunderland, E. M., and Jacob, D. J.: Anthropogenic impacts on global storage and emissions of mercury from terrestrial soils: Insights from a new global model, Journal of Geophysical Research-Biogeosciences, 115, Artn G03008 Doi 10.1029/2009jg001124, 2010.

Soerensen, A. L., Sunderland, E. M., Holmes, C. D., Jacob, D. J., Yantosca, R. M., Skov, H., Christensen, J. H., Strode, S. A., and Mason, R. P.: An Improved Global Model for Air-Sea Exchange of Mercury: High Concentrations over the North Atlantic, Environmental Science & Technology, 44, 8574-8580, Doi 10.1021/Es102032g, 2010.

Stamenkovic, J., and Gustin, M. S.: Nonstomatal versus Stomatal Uptake of Atmospheric Mercury, Environmental Science & Technology, 43, 10.1021/es801583a, 2009.

Streets, D. G., Hao, J. M., Wu, Y., Jiang, J. K., Chan, M., Tian, H. Z., and Feng, X. B.: Anthropogenic mercury emissions in China, Atmospheric Environment, 39, 7789-7806, DOI 10.1016/j.atmosenv.2005.08.029, 2005.

Streets, D. G., Zhang, Q., and Wu, Y.: Projections of Global Mercury Emissions in 2050, Environmental Science & Technology, 43, 2983-2988, Doi 10.1021/Es802474j, 2009.

Strode, S. A., Jaegle, L., Selin, N. E., Jacob, D. J., Park, R. J., Yantosca, R. M., Mason, R. P., and Slemr, F.: Air-sea exchange in the global mercury cycle, Global Biogeochemical Cycles, 21, Artn Gb1017 Doi 10.1029/2006gb002766, 2007.

Sutton, M. A., Nemitz, E., Erisman, J. W., Beier, C., Bahl, K. B., Cellier, P., de Vries, W., Cotrufo, F., Skiba, U., Di Marco, C., Jones, S., Laville, P., Soussana, J. F., Loubet, B., Twigg, M., Famulari, D., Whitehead, J., Gallagher, M. W., Neftel, A., Flechard, C. R., Herrmann, B., Calanca, P. L., Schjoerring, J. K., Daemmgen, U., Horvath, L., Tang, Y. S., Emmett, B. A., Tietema, A., Penuelas, J., Kesik, M., Brueggemann, N., Pilegaard, K., Vesala, T., Campbell, C. L., Olesen, J. E., Dragosits, U., Theobald, M. R., Levy, P., Mobbs, D. C., Milne, R., Viovy, N., Vuichard, N., Smith, J. U., Smith, P., Bergamaschi, P., Fowler, D., and Reis, S.: Challenges in quantifying biosphere-atmosphere exchange of nitrogen species, Environmental Pollution, 150, 125-139, DOI 10.1016/j.envpol.2007.04.014, 2007.

USEPA: User's guide for evaluating subsurface vapor instrusion into buildings (User's Guide), in, Washington, DC: U.S. Environmental Protection Agency, 2004.

Xu, X. H., Yang, X. S., Miller, D. R., Helble, J. J., and Carley, R. J.: Formulation of bi-directional atmosphere-surface exchanges of elemental mercury, Atmospheric Environment, 33, 4345-4355, Doi 10.1016/S1352-2310(99)00245-9, 1999.

Yin, R. S., Feng, X. B., and Meng, B.: Stable Mercury Isotope Variation in Rice Plants (Oryza sativa L.) from the Wanshan Mercury Mining District, SW China, Environmental Science & Technology, 47, 2238-2245, Doi 10.1021/Es304302a, 2013.

Zehner, R. E., and Gustin, M. S.: Estimation of mercury vapor flux from natural substrate in Nevada, Environmental Science & Technology, 36, 4039-4045, Doi 10.1021/Es015723c, 2002.

Zhang, H., and Lindberg, S. E.: Sunlight and iron(III)-induced photochemical production of dissolved gaseous mercury in freshwater, Environmental Science & Technology, 35, 928-935, Doi 10.1021/Es001521p, 2001.

Zhang, L., Brook, J. R., and Vet, R.: A revised parameterization for gaseous dry deposition in air-quality models, Atmospheric Chemistry and Physics, 3, 2067-2082, 2003.

Zhang, L., Wright, L. P., and Blanchard, P.: A review of current knowledge concerning dry deposition of atmospheric mercury, Atmospheric Environment, 43, 5853-5864, 10.1016/j.atmosenv.2009.08.019, 2009a.

Zhang, L., Blanchard, P., Gay, D. A., Prestbo, E. M., Risch, M. R., Johnson, D., Narayan, J., Zsolway, R., Holsen, T. M., Miller, E. K., Castro, M. S., Graydon, J. A., St Louis, V. L., and Dalziel, J.: Estimation of speciated and total mercury dry deposition at monitoring locations in eastern and central North America, Atmospheric Chemistry and Physics, 12, 4327-4340, DOI 10.5194/acp-12-4327-2012, 2012.

Zhang, L. M., Brook, J. R., and Vet, R.: On ozone dry deposition - with emphasis on non-stomatal uptake and wet canopies, Atmospheric Environment, 36, 4787-4799, Pii S1352-2310(02)00567-8 Doi 10.1016/S1352-2310(02)00567-8, 2002a.

Zhang, L. M., Moran, M. D., Makar, P. A., Brook, J. R., and Gong, S. L.: Modelling gaseous dry deposition in AURAMS: a unified regional air-quality modelling system, Atmospheric Environment, 36, 537-560, Doi 10.1016/S1352-2310(01)00447-2, 2002b.

Zhang, L. M., Wright, L. P., and Blanchard, P.: A review of current knowledge concerning dry deposition of atmospheric mercury, Atmospheric Environment, 43, 5853-5864, DOI 10.1016/j.atmosenv.2009.08.019, 2009b.

Zotarelli, L., Dukes, D. M., and Morgan, K. T.: Interpretation of soil moisture content to determine soil field capacuty and avoid over-orrigating sandy soils using soil moisture sensors, The Agricultural and Biological Engineering Department, Florida Cooperative Extension Service, Institute of Food and Agricultural Sciences, University of Florida., AE460, 2010.

663 Table 1. Model variables and units in the base-case simulation

Term	Description	Value or units
F_w	Flux from water bodies	ng m^{-2} hr^{-1}
K_w	Mass transfer coefficient of mercury through water layer	m hr^{-1}
C_w	DGM concentration	40 ng m^{-3} water [a]
H_w	Henry's law constant under water conditions	dimensionless
F_{cnp}	The flux over canopy biomes	ng m^{-2} hr^{-1}
Δt	Time duration	s
R_a	Aerodynamic resistance	s m^{-1}
R_b	Quasi-laminar sub-layer resistance	s m^{-1}
C_{atm}	Atmospheric Hg concentration	ng m^{-3}
χ_{cnp}	The total compensation point	ng m^{-3}
χ_c	Cuticular interfaces compensation point	ng m^{-3}
χ_s	Stomatal interfaces compensation point	ng m^{-3}
χ_g	Soil interfaces compensation point	ng m^{-3}
R_c	cuticular resistance	s m^{-1}
R_s	stomatal resistance	s m^{-1}
R_g	soil diffusion resistance	s m^{-1}
R_{ac}	in-canopy aerodynamic resistance	s m^{-1}
F_{bls}	the flux from bare land soil	ng m^{-3}
$[Hg^0]_{sl}$	elemental mercury content bound to organic matter	ng g^{-1} soil
H	Henry's Law constant in soil condition	dimensionless
f_{oc}	fraction of organic carbon in topsoil (0-5cm)	2% (dimensionless) [b]
K_{oc}	soil organic carbon to water partitioning coefficient	m^3 water g^{-1} organic carbon
$[Hg(II)]_{sl}$	Hg(II) content in the soil	90 ng g^{-1} soil [c]
$R_{g(SO_2)}$	SO_2 soil diffusion resistance	s m^{-1}
$R_{g(O_3)}$	O_3 soil diffusion resistance	s m^{-1}
α_{Hg^0}	Hg^0 scaling factor basing on SO_2	0 (dimensionless) [d]
β_{Hg^0}	Hg^0 scaling factor basing on O_3	0.1 (dimensionless) [e]
LAP	leaf-air partitioning coefficient for Hg^0 between leaves and air	30000 (dimensionless) [f]
$[Hg_c^0]$	$Hg^{0\ content}$ bound to foliar cuticular surface	ng m^{-3} leaf

$[Hg_c^{II+}]$	newly dry deposited Hg(II) residing on cuticular surfaces	ng m^{-2} leaf
$[Hg_{c,DD}^{II+}]$	the total dry deposited Hg(II) loading on cuticular compartment	ng m^{-2} leaf
$[Hg_w^{II+}]$	Hg(II) leaf wash concentration	0.04 ng m^{-2} leaf [g]
f_{rxn}	fraction of Hg(II) potentially photo-reduced to Hg^0	dimensionless
f_{fixed}	fraction of Hg(II) being fixed into tissue	dimensionless
T_l	leaf thickness	0.000152 m [h]
$[Hg_s^0]$	Dissolved elemental mercury in stomatal compartment	ng m^{-3} leaf
$[Hg_{s,DD}^0]$	deposited Hg^0 concentration stored inside stomatal compartment	0.39 ng m^{-2} leaf hr^{-1} [i]
R_{st}	resistance associating stomata apertures	s m^{-1}
R_{me}	resistance associating mesophyll reservoir	s m^{-1}
W_{st}	fraction of stomatal blocking under wet condition	dimensionless

[a] Value for base-case simulation, Xu et al. (1999);

[b] For 0-20 cm topsoil, the bulk density is 1.1-1.3 g cm^{-3} and organic carbon content is 3.3 kg m^{-2} in the US (Calhoun et al., 2001;Guo et al., 2006), so assuming in the 0-5 cm topsoil foc is 2%;

[c] Value for base-case simulation, Bash (2010) ;

[d] Basing on the negligible solubility (*Henry's constant*=0.139 M atm^{-1}) and chemical inertness (Zhang et al., 2009b;Zhang et al., 2012) ;

[e] Zhang et al. (2012);

[f] Rutter et al. (2011a);

[g] Value for base-case simulation, Frescholtz et al. (2003);

[h] Value for base-case simulation, Abrams and Kubiske (1990);

[i] Value for base-case simulation, Poissant et al. (2008).

675 Table 2. Examined model variables and the experimental levels of factorial design for air-water exchange

Term	Description	Low level	High level
T	Sea surface temperature (°C)	-2 [a]	35 [a]
GEM	Air Hg^0 concentration (ng m^3)	1.0 [b]	2.0 [b]
DGM	Dissolved Hg^0 concentration in surface water(ng m^{-3})	15 [c]	240 [c]
W	Wind speed at 10 m above water surface (m s^{-1})	0.001[d]	20 [d]

676 [a] Kwun and You (2009);

677 [b] According to global background of air Hg^o at 1.1~1.7 ng m^3 (Lindberg et al., 2007);

678 [c] Morel et al. (1998);

679 [d] Andersson et al. (2011).

680 Table 3. Examined model variables and the experimental levels of factorial design for air-soil exchange
681 over sparsely vegetated land, bare ground tundra and snow/ice land
682

Term	Description	Low level	High level
T	Air temperature at 2 meters (°C)	-2	40
Q2	Water vapor mixing ratio (Kg Kg^{-1})	0.0005 [a]	0.05 [a]
f_{oc}	Fraction of organic carbon in surface soil	0.006 [b]	0.1[c]
UST	Friction velocity(m s^{-1})	0.0001[d]	1.0 [d]
SM	Soil Hg content (ng g^{-1} soil)	50 [e]	1000 [e]
GEM	Air Hg^0 concentration (ng m^{-3})	1.0	2.0
SNOWH	Snow depth (m)	0 [f]	0.4999 [f]
β_{Hg0}	Scaling factor of reactivity Hg	0.1[g]	0.2 [h]
DC	Dew condition	No [i]	Yes [i]
RC	Rain condition	No [j]	Yes [j]
MC	Moist soil condition	No [k]	Yes [k]

683 [a] Kwun and You (2009);
684 [b] Suggested default value for modeling of volatilized contaminant to air by USEPA (2004);
685 [c] Upper limit of the forest soils (Jones et al., 2004);
686 [d] Akkarappuram and Raman (1988)
687 [e] Carpi and Lindberg (1998);
688 [f] Has effect on ground and cuticular resistance, Zhang et al. (2003);
689 [g] Zhang et al. (2012) ;
690 [h] Zhang et al. (2009a) ;
691 [i] Air temperature below dew point represents low level and vice versa, has effect on ground and cuticular
692 resistance (Zhang et al., 2003);
693 [j] Has effect on ground and cuticular resistance terms (Zhang et al., 2003) ;
694 [k] Soil moisture > 20% represents low level and vice versa, the high level suggests highly moist soil
695 (Zotarelli et al., 2010).

Table 4. Examined model variables and the experimental levels of factorial design for air-canopy exchange

Term	Description	Low level	High level
T	Air temperature at 2 meters (°C)	-2	40
f_{oc}	Fraction of organic carbon in surface soil	0.006	0.1
UST	Friction velocity(m s^{-1})	0.0001	1.0
SM	Soil total Hg content (ng m^{-3})	50	1000
β_{Hg0}	Scaling factor of reactivity Hg	0.1	0.2
SNOWH	Snow depth (m)	0	0.4999
LAI	Leaf area index (m^2 m^{-2})	1.0 [a]	5.0 [a]
SR	Solar irradiation (W m^{-2})	0	1000
Leaf_Hg	Hg concentration in leaf rinse (ng m^{-2} leaf)	0.02 [b]	2.10 [c]
Stomata_Hg	Hg previously deposited to leaf stomata (ng m^{-2} leaf)	0.13 [d]	0.59 [d]
GEM	Air Hg^0 concentration (ng m^{-3})	1.0	2.0
LAP	Leaf-air partitioning coefficient (m^3 air m^{-3} leaf)	30000 [e]	6000000 [e]
DC	Dew condition	No	Yes
RC	Rain condition	No	Yes
MC	Moist soil condition	No	Yes

[a] Gower et al. (1999)

[b] Frescholtz et al. (2003)

[c] Fay and Gustin (2007)

[d] Poissant et al. (2008)

[e] Rutter et al. (2011)

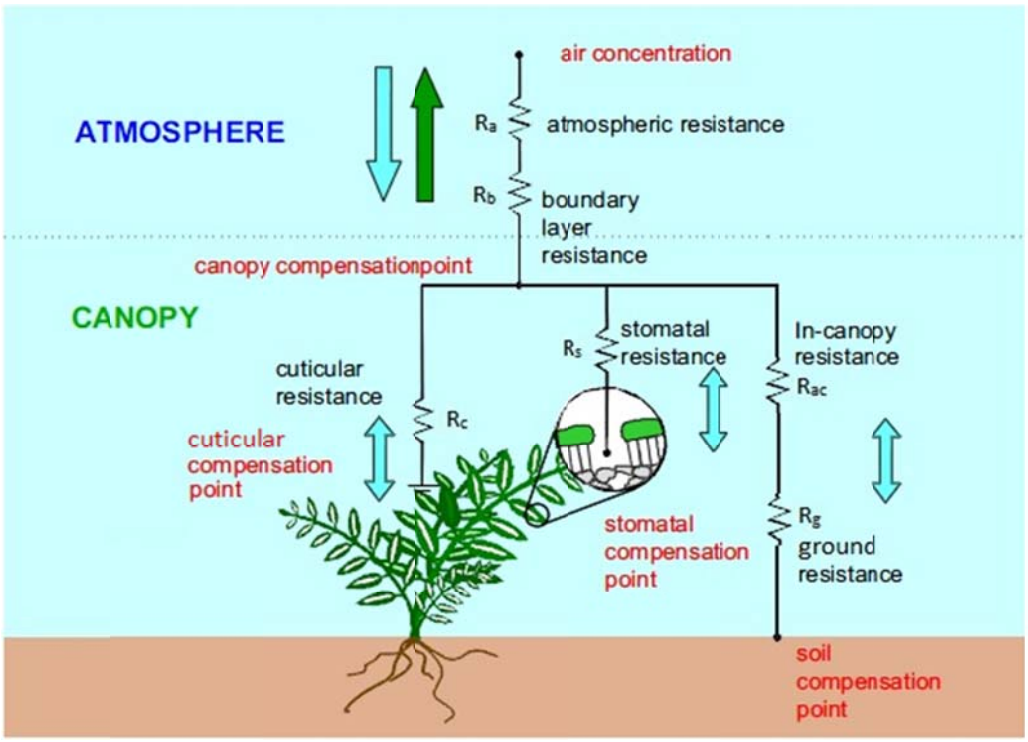

Figure 1. Resistance scheme implemented in the air-surface exchange model following Sutton et al. (2007) and Zhang et al. (2009a)

706

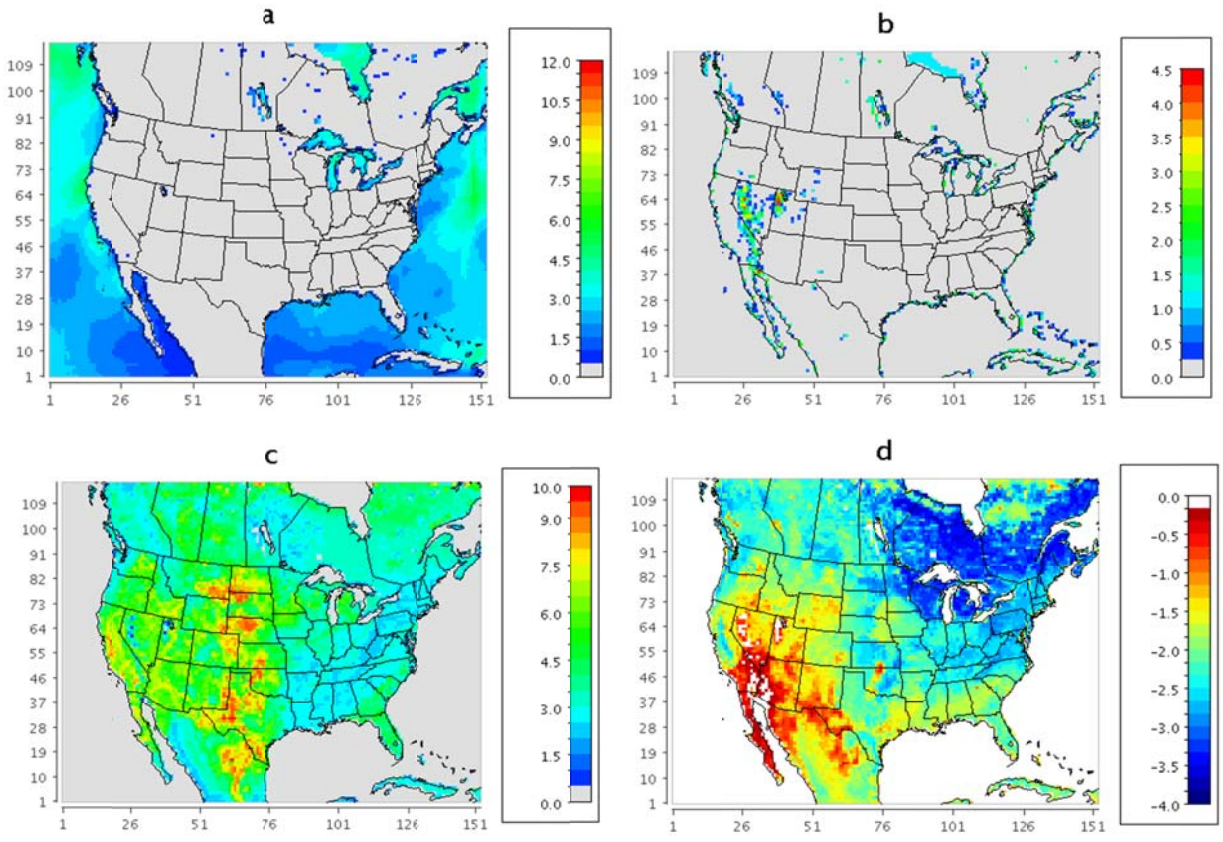

707

708 Figure 2. Monthly mean of the simulated Hg^0 flux (ng m^{-2} hr^{-1}) in the summer month: (a) flux from water

709 body, (b) flux from bare lands, (c) flux from soil under the canopy, and (d) flux from foliage.

710

711

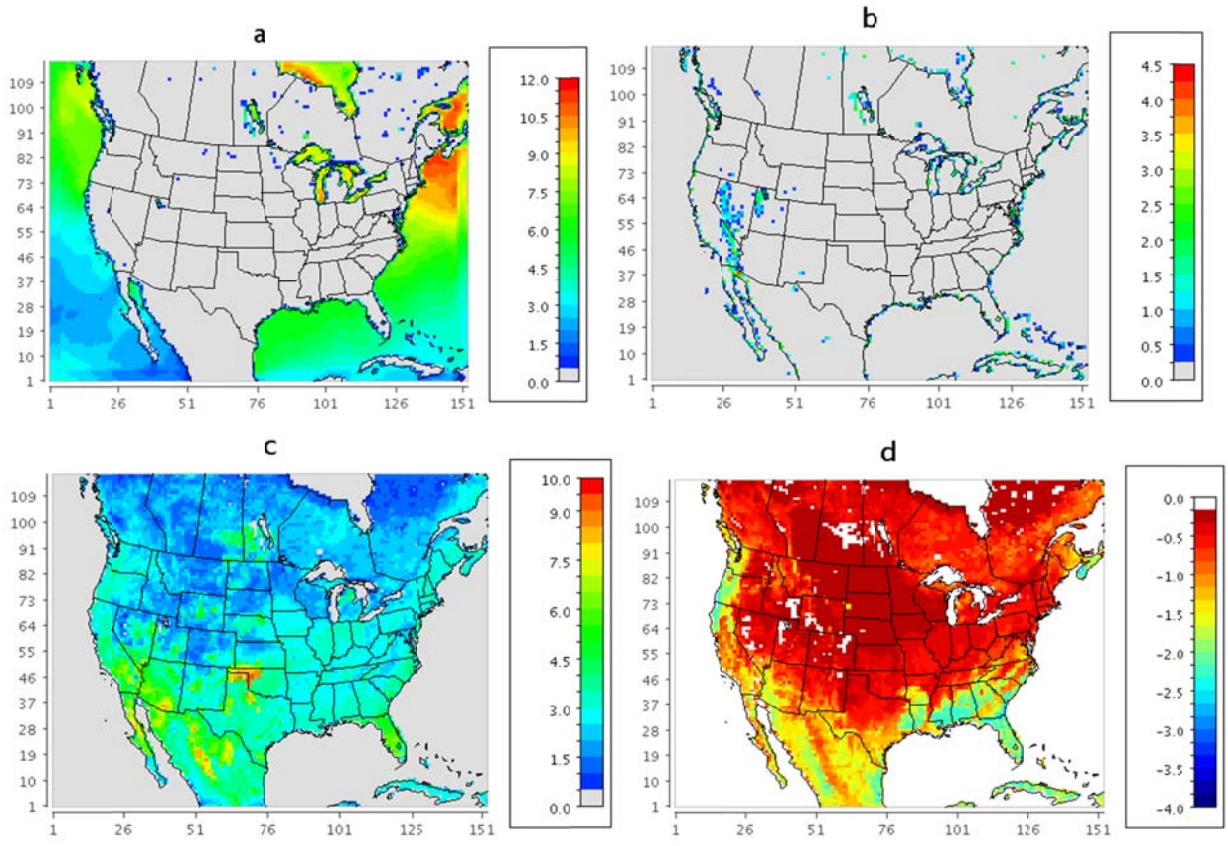

712

713 Figure 3. Monthly mean of the simulated Hg^0 flux (ng m^{-2} hr^{-1}) in the winter month: (a) flux from water

714 body, (b) flux from bare lands, (c) flux from soil under the canopy, and (d) flux from foliage.

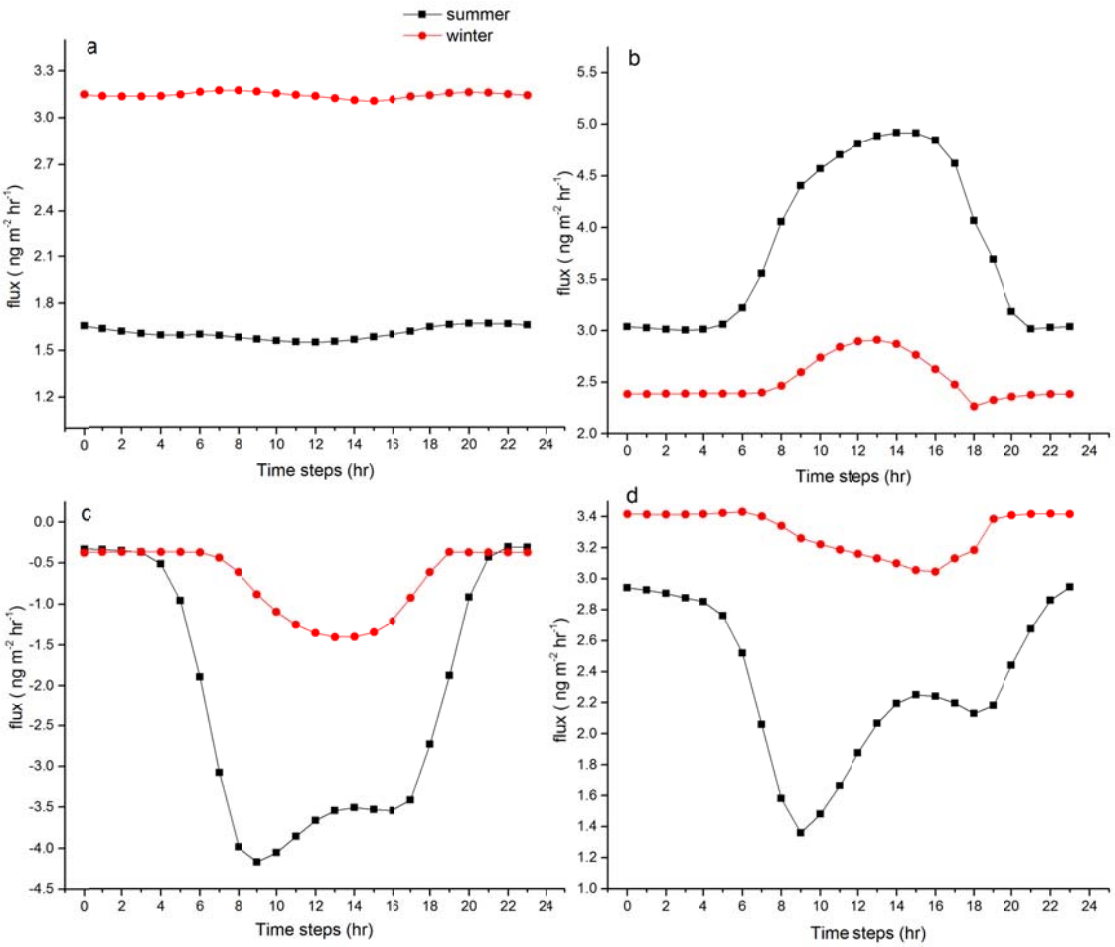

715

716 Figure 4. Diurnal variation of mean simulated Hg^0 for the entire model domain (UTC-7): (a) flux from

717 water body, (b) total flux from soils (soil under the canopy and bare lands), (c) flux from foliage, and (d)

718 flux for the total domain.

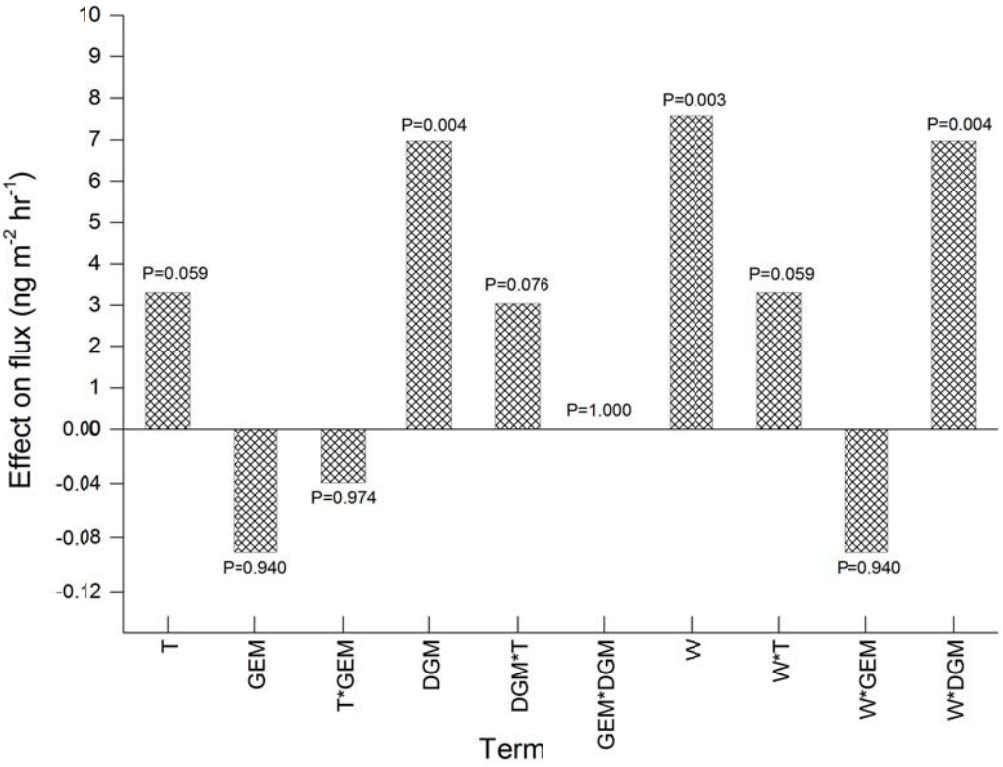

719

720 Figure 5. Sensitivity analysis based on the 2^4 factorial design shown in Table 2 (water body). T denotes
721 air temperature at water surface; GEM denotes air Hg concentration; DGM denotes dissolved gaseous Hg
722 concentration in surface water; W denotes wind speed. "*" denotes the interaction effects.

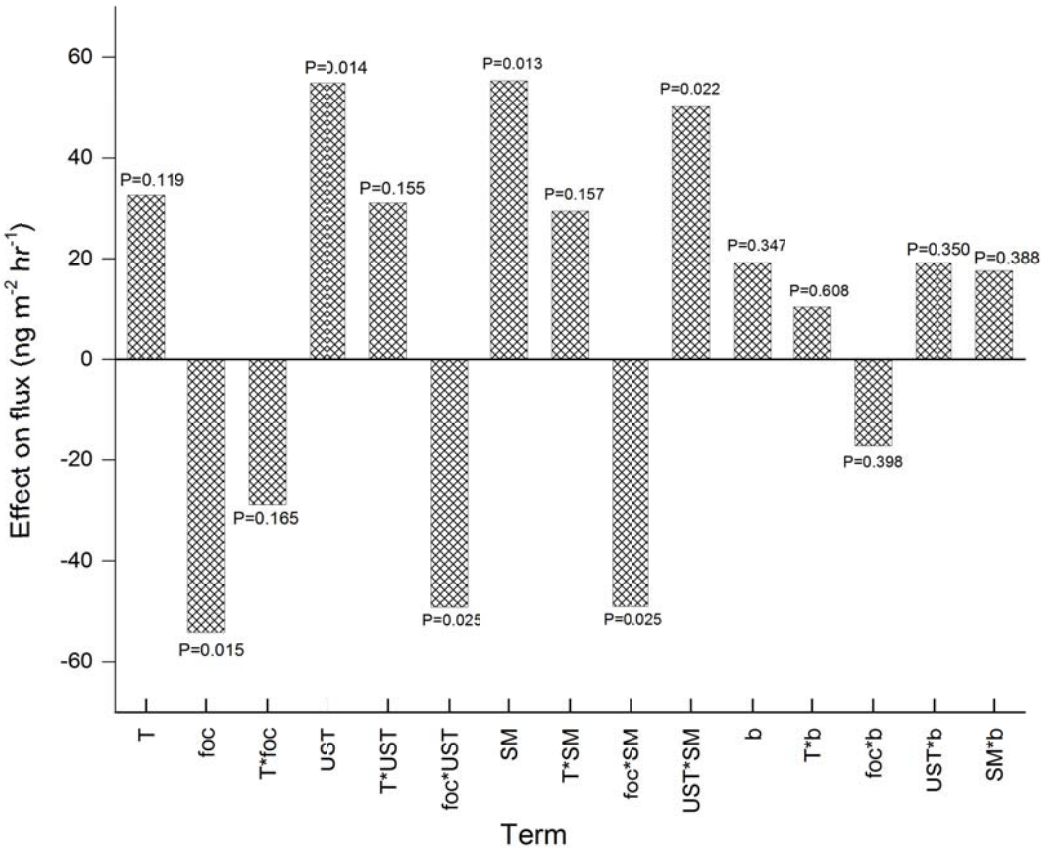

723

724 Figure 6. Sensitivity analysis based on the 2^5 factorial design for bare lands after pre-screening model

725 variables shown in Table 3 to isolate the significant factors. T denotes surface air temperature; foc

726 denotes fraction of organic carbon in soil; UST denotes friction velocity; SM denotes soil mercury

727 content; b denotes scaling factor for Hg reactivity (β_{Hg0}). "*" denotes interaction effects.

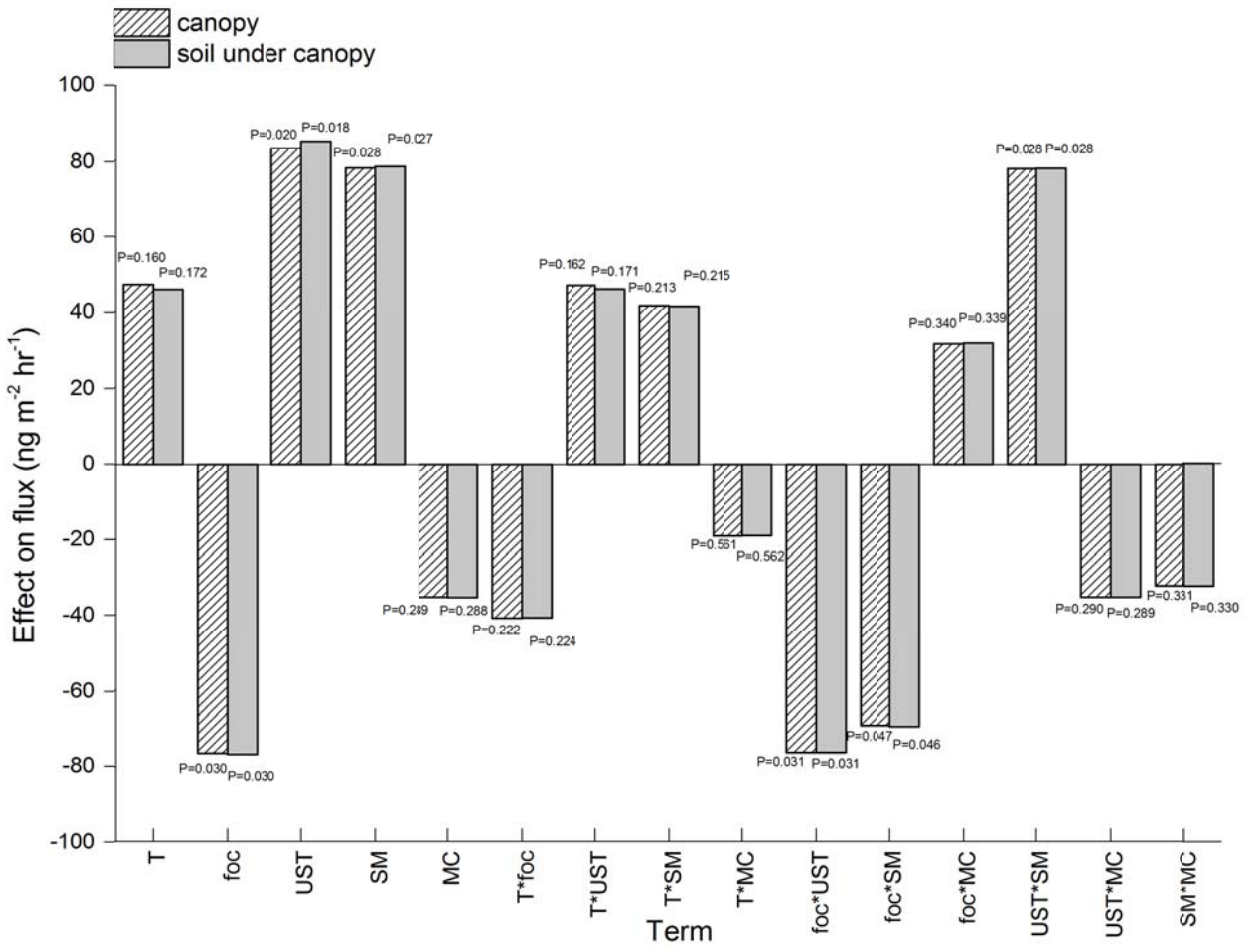

Figure 7. Sensitivity analysis based on the 2^5 factorial design at canopy level after pre-screening model variables shown in Table 4 to isolate the significant factors. The overall flux at canopy level is dominated by the soil flux under the canopy (the sensitivity of foliar exchange is shown in Figure 8). T denotes surface air temperature; foc denotes fraction of organic carbon in soil; UST denotes friction velocity; SM denotes soil Hg content; MC denotes soil moisture. "*" denotes interaction effects.

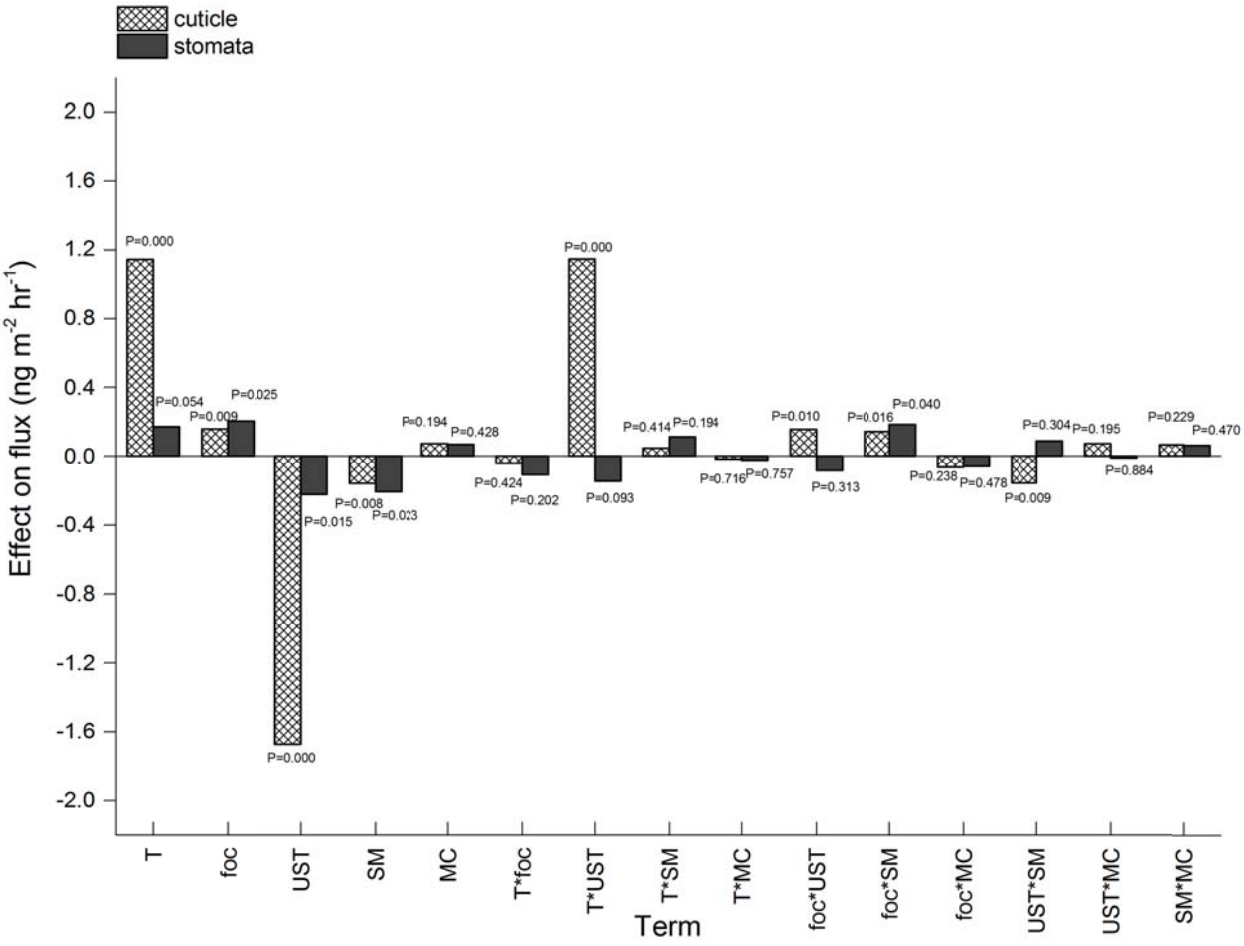

734

735 Figure 8. Sensitivity analysis based on the 2^5 factorial design for foliar exchange after pre-screening

736 model variables shown in Table 4 to isolate the significant factors. T denotes surface air temperature; foc

737 denotes fraction of organic carbon in soil; UST denotes friction velocity; SM denotes soil Hg content;

738 MC denotes soil moisture. "*" denotes interaction effects.

Supplementary Material: Sensitivity analysis of an updated bidirectional air-surface exchange model for mercury vapor

Xun Wang[1,2], Che-Jen Lin[1,3,4], Xinbin Feng[1]

[1] State Key Laboratory of Environmental Geochemistry, Institute of Geochemistry, Chinese Academy of Sciences, Guiyang, China

[2] University of Chinese Academy of Sciences, Beijing, China

[3] Department of Civil Engineering, Lamar University, Beaumont, TX, USA

[4] College of Environment and Energy, South China University of Technology, Guangzhou, China

Correspondence to: C.-J. Lin (jerry.lin@lamar.edu); X. Feng (fengxinbin@vip.skleg.cn)

1. Use of 2^{k-p} factorial design for

Design of experiments is a series of tests in which purposeful changes are made to the input variables of a process systematically and the effects on response variables are measured. It is widely applied in the experiments involving many influencing factors, when it is necessary to study the combined effect of these factors. For a two-level design involving a high-level and a low-level value for each factor, the number of all possible combinations is 2^k (for example, for two factors the combinations is low-low, low-high, high-low and high-high), which also represent the number of experiments. This exponential relationship rapidly increases the number of experiments when the number of studied factors is increased. To reduce the experimental effort without losing the analytical power of the experiments, the number of experiment can be decreased strategically by choosing the experiments that investigate the main effects (i.e., the effect of single factor) and interaction effects of lower order. This is called fractional design and the number of experiment can be reduced by 2^p times (i.e., the number of experiment becomes 2^{k-p}). The term “Resolution” is used by statisticians to indicate how the experiments are chosen. For IV resolution design, all the main effects are completely isolated from confounding with

all other experimental runs and the second-order (two-factor) interactions are maintained without confounding with higher order interactions. Based on the factorial experiment results, statistical test can be performed to understand the significance of each factor using P value.

An excellent online presentation on factorial design of experiments is also available at http://www.jhuapl.edu/techdigest/td/td2703/telford.pdf.

2. Initial parameter screening for bare lands

Normal plot of the standardized effects of 2^{11-6} (Figure s1) suggests significant effect from fraction of organic carbon, friction velocity, soil Hg content at 95% confidence level. The P-value of main effects from air temperature at 2 meters and scaling factor for reactivity of mercury on ozone (β_{Hg^0}) were close to 0.05 (0.069 and 0.073, respectively). For the second order interactions, air temperature and β_{Hg^0} are important. Therefore fraction of organic carbon, friction velocity, soil Hg concentration, air temperature, β_{Hg^0}, were chosen for the final 2^5 full factorial design.

3. Initial parameter screening for canopy system

The alias structure of the 2^{15-9} fractional design is complex (Figure s2). To ensure that the most significant factors are selected for the final full factorial design, all parameters confounded in alias system were chosen to run 2^{11-6} experiment except for air Hg^0 concentration because its weak significance (P = 0.437). From the results of the 2^{11-6} fractional design (Figure s3) result, the fraction of organic carbon, friction velocity, soil Hg concentration, β_{Hg^0}, soil moisture condition are significant. The P-value of main effects from Hg previously deposited to leaf stomata and air temperature were close to 0.05 (0.069 and 0.136, respectively). Therefore, fraction of organic carbon, friction velocity, soil Hg concentration, β_{Hg^0}, soil under moisture condition, Hg previously deposited to leaf stomata and air temperature were chosen to for another 2^{7-1} fractional

experiments. Based on the results (Figure s7), the main effects from fraction of organic carbon, friction velocity, soil Hg concentration are significant. To get the full design, Hg previously deposited to leaf stomata and β_{Hg^0} were eliminated because of the relatively weaker significance.

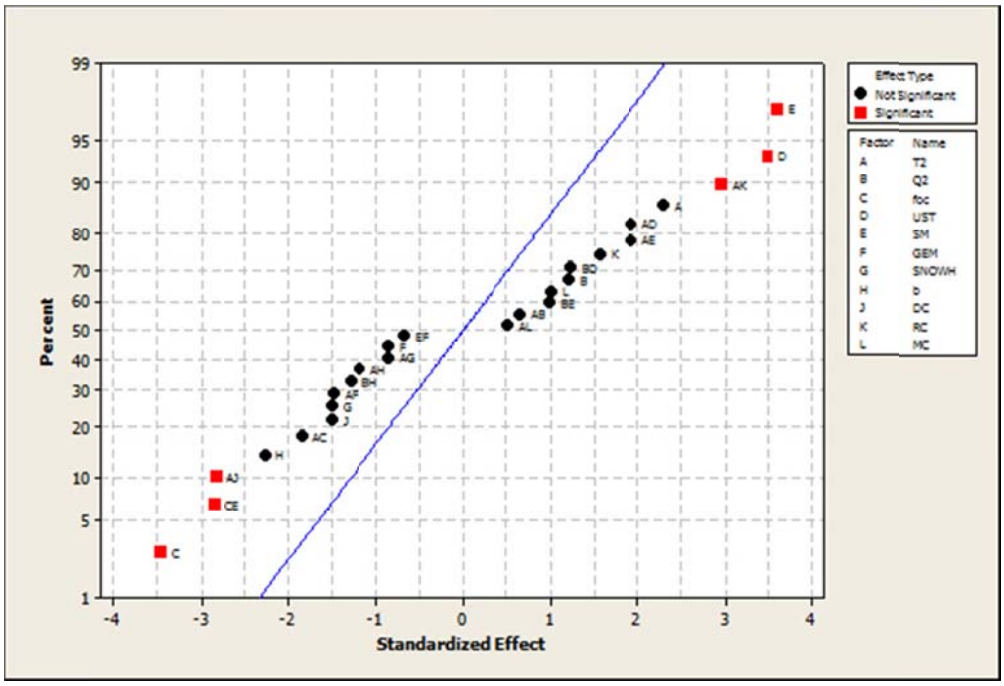

Figure s1: Results of 2^{11-6} fractional design for bare lands. Significance at P<0.05. T denotes air temperature at 2 meters, Q2 denotes water vapor mixing ratio, foc denotes fraction of organic carbon in surface soil, UST denotes friction velocity, SM denotes soil total Hg concentration, GEM denotes air Hg(0) concentration, SNOWH denotes snow depth, b denotes scaling factor of reactivity Hg, DC denotes dew condition, RC denotes rain condition, MC denotes moist soil condition. Alias information for significant terms: T*DC + Q2*SNOWH + foc*UST + SM*b, T*RC + Q2*MC+ foc*b + UST*SM, foc*SM + UST*b + SNOWH*MC + DC*RC.

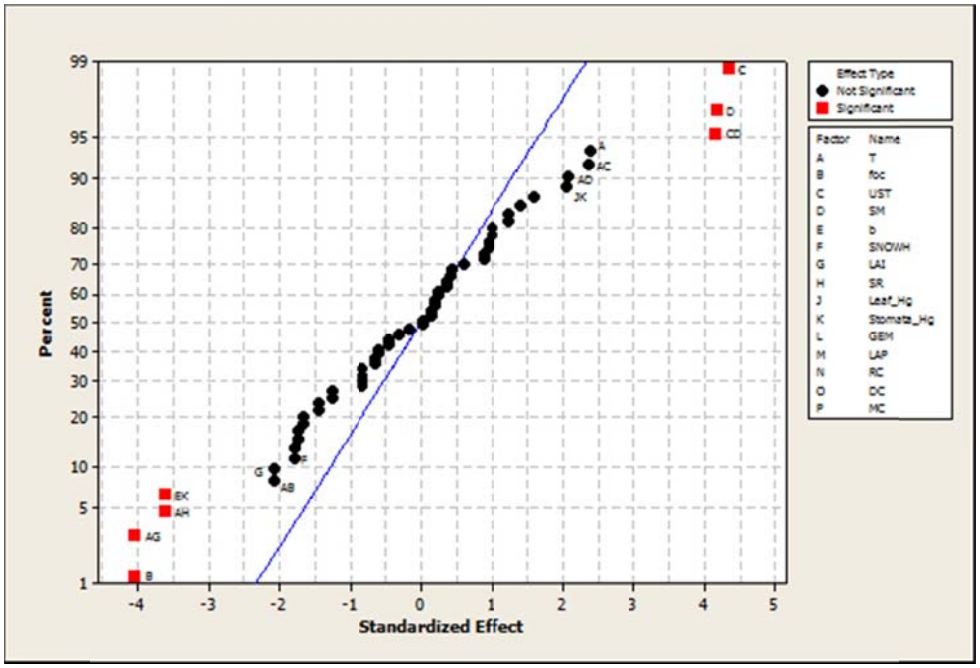

Figure s2: Results of 2^{15-9} fractional design for canopy system. Significance at P<0.05. T denotes air temperature at 2 meters, foc denotes fraction of organic carbon in surface soil, UST denotes friction velocity, SM denotes soil total Hg concentration, b denotes scaling factor of reactivity Hg, SNOWH denotes snow depth, LAI denotes Leaf area index , SR denotes solar irradiation, Leaf_Hg denotes Hg concentration in leaf rinse, Stomata_Hg denotes Hg previously deposited to leaf stomata, GEM denotes air Hg(0) concentration, LAP denotes leaf-air partitioning coefficient, DC denotes dew condition, RC denotes rain condition, MC denotes moist soil condition. Alias information for significant terms: T*LAI + foc*UST, T*SR + foc*SM, UST*SM + LAI*SR + GEM*LAP, b*Stomata_Hg + RC*MC.

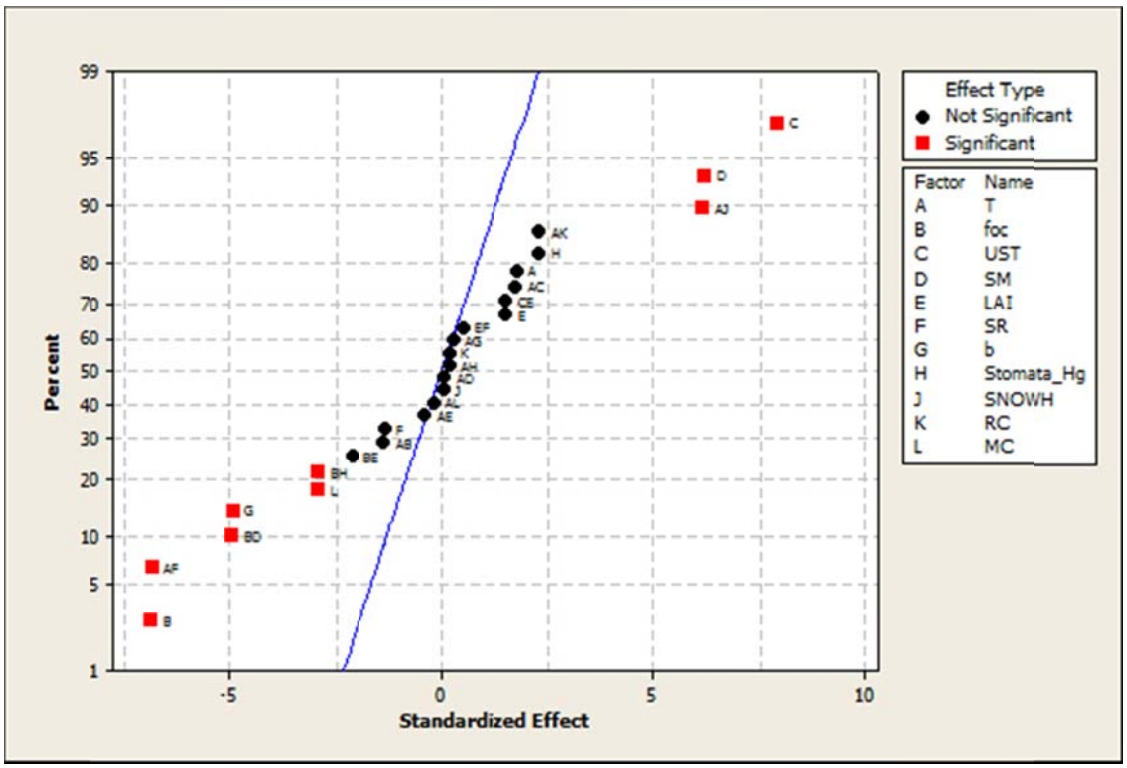

Figure s3: Results of 2^{11-6} fractional design for canopy system. Significance at P<0.05. T denotes air temperature at 2 meters, foc denotes fraction of organic carbon in surface soil, UST denotes friction velocity, SM denotes soil total Hg concentration, LAI denotes leaf area index, SR denotes solar irradiation, b denotes scaling factor of reactivity Hg, Stomata_Hg denotes Hg previously deposited to leaf stomata, SNOWH denotes snow depth, RC denotes rain condition, MC denotes moist soil condition. Alias information for significant terms: T*SR + foc*UST + SM*b + Stomata_Hg*MC, T*SNOWH + foc*b + UST*SM + LAI*Stomata_Hg, foc*LAI + SM*MC + b*Stomata_Hg, foc*Stomata_Hg + UST*MC + LAI*b + SR*RC.

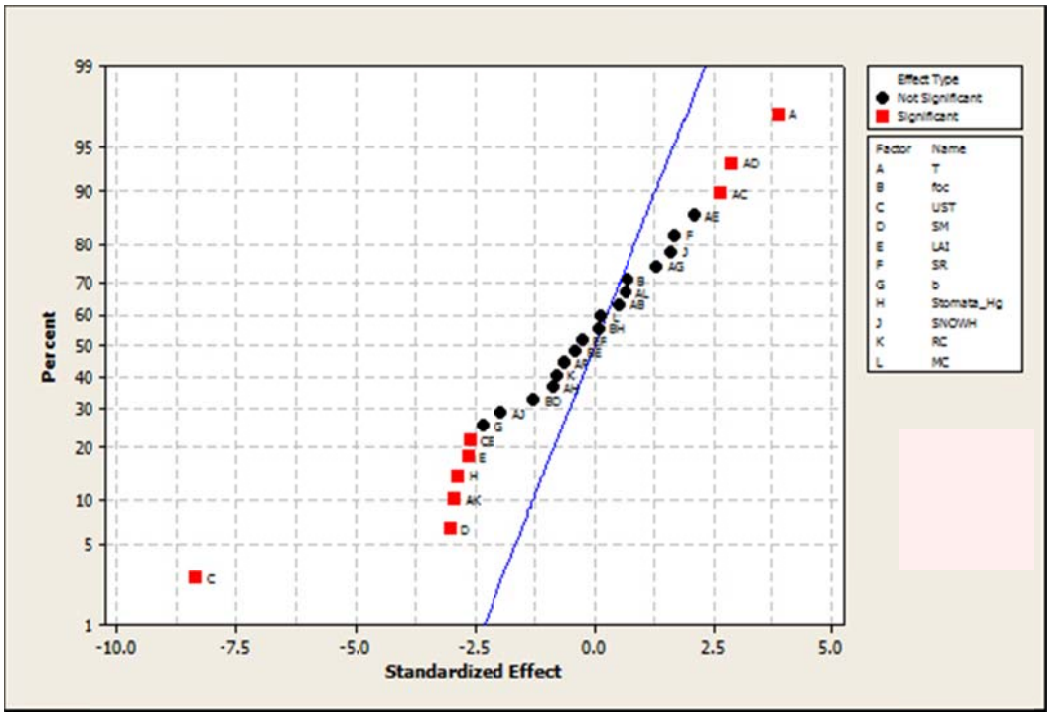

Figure s4: Results of 2^{11-6} fractional design for foliage. Significance at P<0.05. T denotes air temperature at 2 meters, foc denotes fraction of organic carbon in surface soil, UST denotes friction velocity, SM denotes soil total Hg concentration, LAI denotes leaf area index, SR denotes solar irradiation, b denotes scaling factor of reactivity Hg, Stomata_Hg denotes Hg previously deposited to leaf stomata, SNOWH denotes snow depth, RC denotes rain condition, MC denotes moist soil condition. Alias information for significant terms: T*SR + foc*UST + SM*b + Stomata_Hg*MC, T*SNOWH + foc*b + UST*SM + LAI*Stomata_Hg, foc*LAI + SM*MC + b*Stomata_Hg, foc*Stomata_Hg + UST*MC + LAI*b + SR*RC.

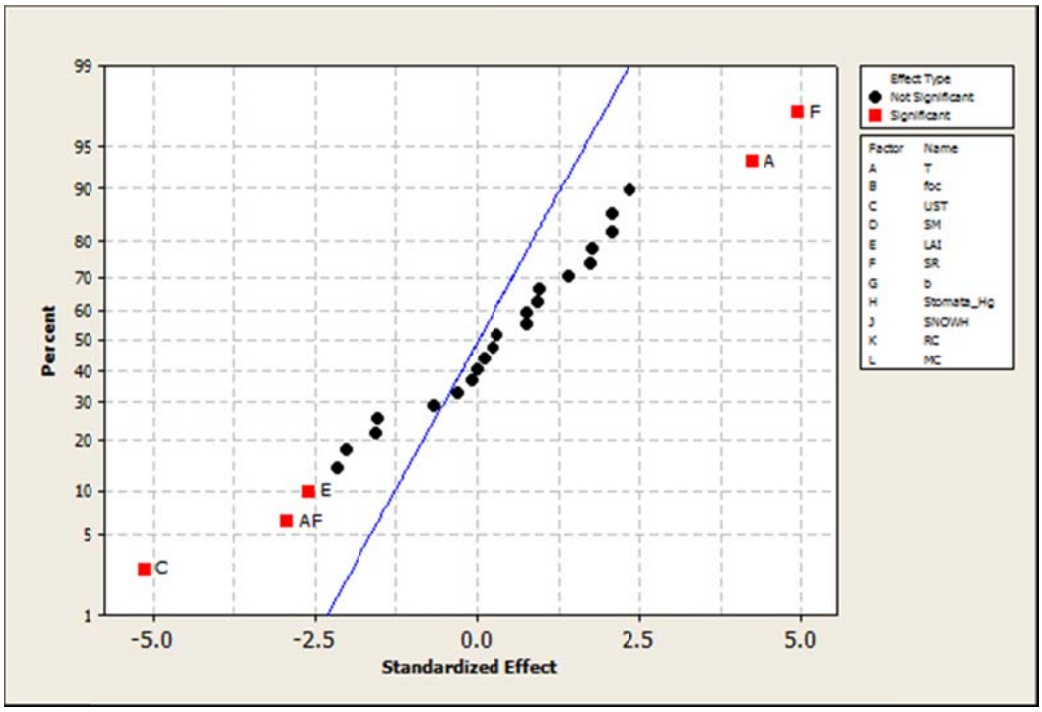

Figure s5: Results of 2^{11-6} fractional design for cuticle. Significance at P<0.05. T denotes air temperature at 2 meters, foc denotes fraction of organic carbon in surface soil, UST denotes friction velocity, SM denotes soil total Hg concentration, LAI denotes leaf area index, SR denotes solar irradiation, b denotes scaling factor of reactivity Hg, Stomata_Hg denotes Hg previously deposited to leaf stomata, SNOWH denotes snow depth, RC denotes rain condition, MC denotes moist soil condition. Alias information for significant terms: T*SR + foc*UST + SM*b + Stomata_Hg*MC, T*SNOWH + foc*b + UST*SM + LAI*Stomata_Hg, foc*LAI + SM*MC + b*Stomata_Hg, foc*Stomata_Hg + UST*MC + LAI*b + SR*RC.

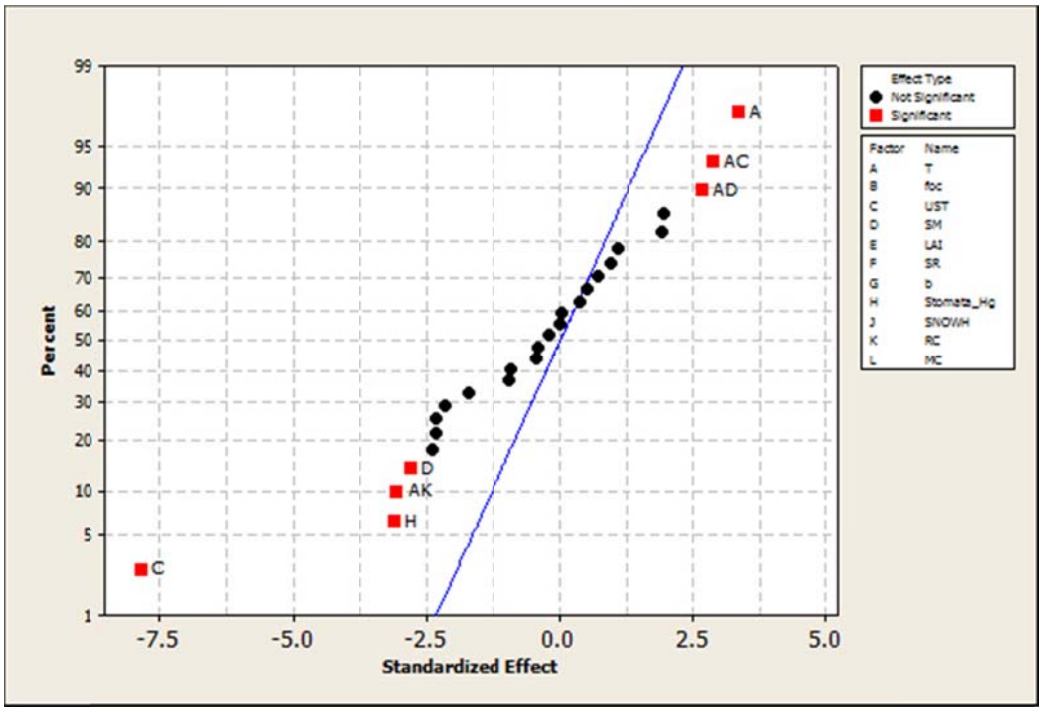

Figure s6: Results of 2^{11-6} fractional design for stamata. Significance at P<0.05. T denotes air temperature at 2 meters, foc denotes fraction of organic carbon in surface soil, UST denotes friction velocity, SM denotes soil total Hg concentration, LAI denotes leaf area index, SR denotes solar irradiation, b denotes scaling factor of reactivity Hg, Stomata_Hg denotes Hg previously deposited to leaf stomata, SNOWH denotes snow depth, RC denotes rain condition, MC denotes moist soil condition. Alias information for significant terms: T*SR + foc*UST + SM*b + Stomata_Hg*MC, T*SNOWH + foc*b + UST*SM + LAI*Stomata_Hg, foc*LAI + SM*MC + b*Stomata_Hg, foc*Stomata_Hg + UST*MC + LAI*b + SR*RC.

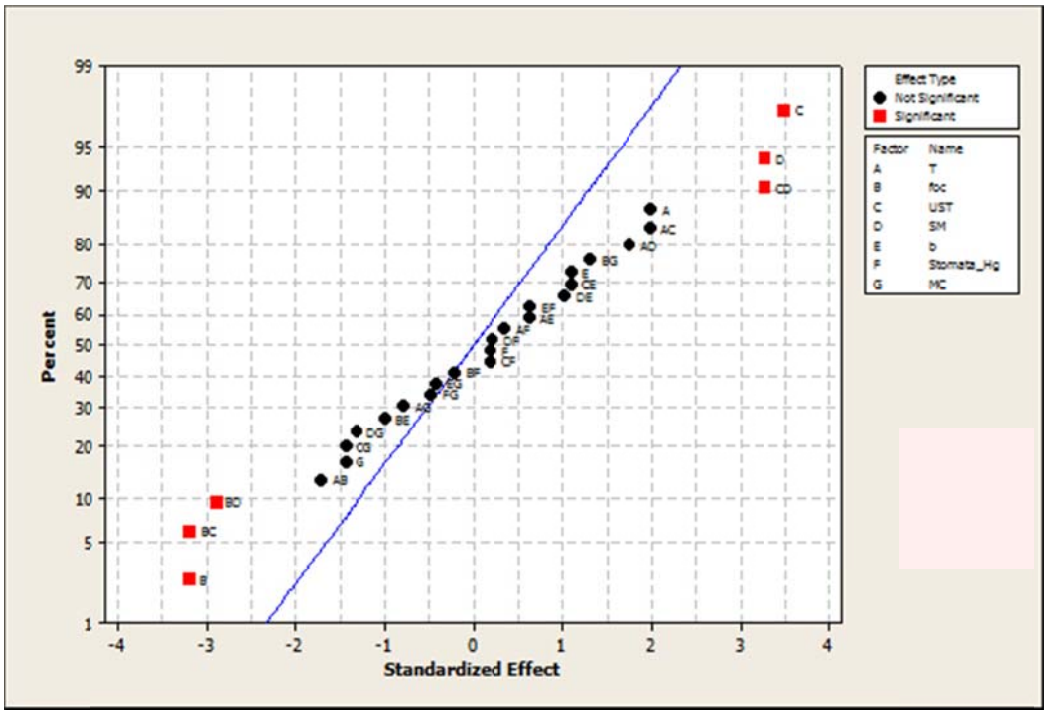

Figure s7: Results of 2^{7-1} fractional design for canopy system. Significance at P<0.05. T denotes air temperature at 2 meters, foc denotes fraction of organic carbon in surface soil, UST denotes friction velocity, SM denotes soil total Hg concentration, MC denotes moist soil condition. Alias information for significant terms: T*SR + foc*UST + SM*b + Stomata_Hg*MC, T*SNOWH + foc*b + UST*SM + LAI*Stomata_Hg, foc*LAI + SM*MC + b*Stomata_Hg, foc*Stomata_Hg + UST*MC + LAI*b + SR*RC.

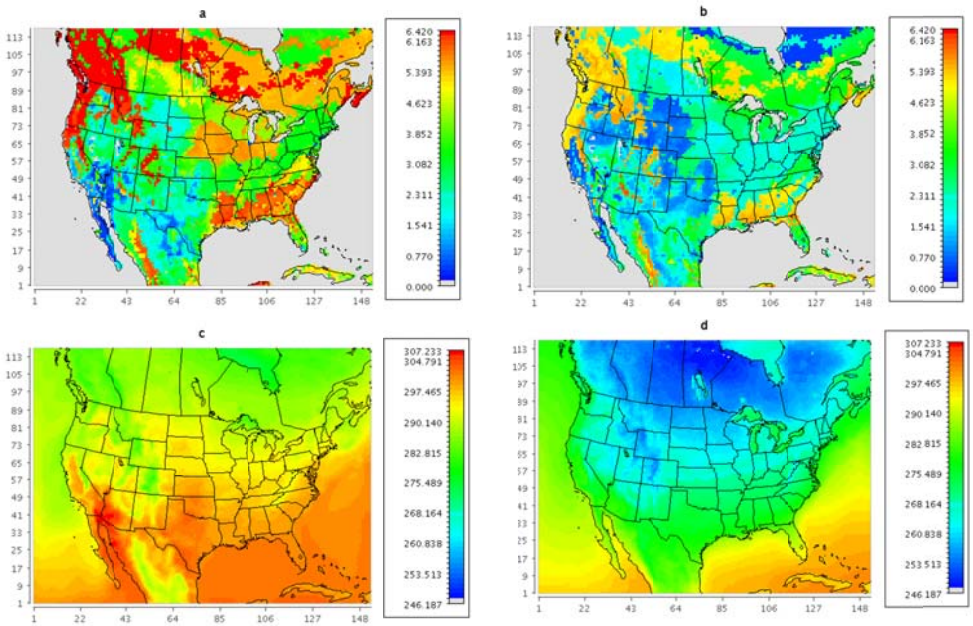

Figure s8: (a) the average spatial distribution of LAI (m^2 m^{-2}) in the summer month; (b) the average spatial distribution of LAI (m^2 m^{-2}) in the winter month; (c) the average spatial distribution of air temperature at 2 meters (K) in the summer month; (d) the average spatial distribution of air temperature at 2 meters (K) in the winter month